

# Catalog of Galaxy Morphology in Four Rich Clusters : Luminosity Evolution of Disk Galaxies at $0.33 < z < 0.83$ <sup>1</sup>

Amélie Saintonge<sup>2</sup>, David Schade

*Dominion Astrophysical Observatory, Herzberg Institute of Astrophysics, National Research  
Council of Canada, Victoria, BC, V9E 2E7, Canada*

E. Ellingson

*Center for Astrophysics and Space Astronomy, University of Colorado, Boulder, CO, 80309*

H.K.C. Yee and R. G. Carlberg

*Department of Astronomy, University of Toronto, Toronto, ON, M5S 3H8, Canada*

## ABSTRACT

*Hubble Space Telescope* (HST) imaging of four rich, X-ray luminous, galaxy clusters ( $0.33 < z < 0.83$ ) is used to produce quantitative morphological measurements for galaxies in their fields. Catalogs of these measurements are presented for 1642 galaxies brighter than  $F814W(AB)=23.0$ . Galaxy luminosity profiles are fitted with three models: exponential disk, de Vaucouleurs bulge, and a disk-plus-bulge hybrid model. The best fit is selected and produces a quantitative assessment of the morphology of each galaxy: the principal parameters derived being  $B/T$ , the ratio of bulge to total luminosity, the scale lengths and half-light radii, axial ratios, position angles and surface brightnesses of each component. Cluster membership is determined using a statistical correction for field galaxy contamination, and a mass normalization factor (mass within boundaries of the observed fields) is derived for each cluster. Morphological classes are defined using  $B/T$ : disk galaxies have  $0 \leq B/T \leq 0.4$ , intermediate galaxies  $0.4 < B/T < 0.8$ , and bulge-dominated galaxies have  $0.8 \leq B/T \leq 1$ . In the present paper, this catalog of measurements is used to investigate the luminosity evolution of disk galaxies in the rich-cluster environment. Examination of the relations between disk scale-length and central surface brightness suggests, under the assumption that these clusters represent a family who share a common evolutionary history and are simply observed at different ages, that there is a dramatic change in the properties of the small disks ( $h < 2$  kpc). This change is best characterized as a change in surface brightness by  $\sim 1.5$  magnitude between  $z = 0.3$  and  $z = 0.8$  with brighter disks at higher redshifts.

*Subject headings:* galaxies: evolution, galaxies: spiral, galaxies: clusters: individual (MS 1358.4+6245, MS0015.9+1609, MS 1621.5+2640, MS 1054.4-0321)

## 1. INTRODUCTION

Because of their extreme environments, clusters are interesting places in which to study galaxy evolution (Dressler 1984; Martel, Premade, & Matzner 1998). Their cores have the highest volume density of galaxies in the Universe so that any environmental dependence of galaxy formation or evolution processes should be most pronounced there, when contrasted with studies of the field population. A more pedestrian motivation for studying galaxies in clusters is that the high surface density of objects makes them easy targets for imaging and multi-object spectroscopy. Reasonably well-selected samples of clusters are now available up to redshift approaching  $z = 1$  (e.g. Rosati et al. (1998); Gladders, Yee, & Ellingson (2002)). However, it could be argued that the sample of well-studied clusters (those with high-resolution imaging, morphological measurements, and extensive spectroscopy) is still fairly small. The small sample means that, if galaxy clusters are a diverse population (in terms of richness, X-ray luminosity, behavior of galaxy populations), then it will be difficult to draw the correct general conclusions from studying the present sample. Furthermore, it is difficult to trace the pedigree of the sample of clusters that has been well-studied to this date. By this we mean that a complex and tangled process of selection has been applied to broader samples of clusters and that process results in the well-studied sample that presently exists. If, for example, a cluster was chosen for extensive spectroscopy because of the presence of a large fraction of blue galaxies, and then chosen for HST imaging because it had a large population of emission-line galaxies, then this cluster cannot be claimed to be a member of a representative set of clusters. Conclusions drawn from a sample with this type of pre-selection for detailed study will not be generally applicable. The CNOC (Yee, Ellingson & Carlberg 1996) sample of clusters was chosen by X-ray luminosity and redshift and should avoid some of these potential problems.

The phenomenology of galaxy populations in clusters can be divided roughly (and perhaps not physically) into five areas. The first is the formation and evolution of elliptical galaxies which dominate the core of clusters (Hubble & Humason 1931) and which may

---

<sup>1</sup>Based on observations obtained with the NASA/ESA *Hubble Space Telescope*, which is operated by STScI for the Association of Universities for Research in Astronomy, Inc., under NASA contract NAS5-26555.

<sup>2</sup>Current address: Center for Radiophysics and Space Research, Cornell University, Space Sciences Building, Ithaca, NY 14853; [amelie@astro.cornell.edu](mailto:amelie@astro.cornell.edu)

have been in place prior to cluster virialization (Dressler et al. 1997). Ellipticals seem to form the backbone of the cluster galaxy population. In local clusters they show a very tight color-magnitude relation with small scatter which implies either an early formation epoch or synchronization of formation times (Bower, Lucey, & Ellis 1992). Nearby ellipticals follow a tight fundamental plane relation between size, surface brightness, and velocity dispersion (Djorgovski & Davis 1987; Dressler et al. 1987). The tightness of the cluster color-magnitude relation seems to be preserved (Ellis et al. 1997) to  $z \sim 0.5$  placing tighter constraints on the formation epoch. Studies of the moderate redshift fundamental plane (van Dokkum et al. 1998b; Kelson et al. 1997) and the relation between size and luminosity (Schade, Barrientos, & Lopèz-Cruz 1997), a projection of the fundamental plane, indicate that cluster ellipticals are evolving passively to  $z \sim 1$ , that is, their stellar populations are aging with little ongoing star formation. The data that are available at the present time indicate that all ellipticals in all clusters that have been studied evolve in a similar fashion. Interestingly, cluster and field elliptical populations seem to evolve in an identical manner (Schade et al. 1999).

The second observed cluster phenomenon is the morphology-density relation or morphology-clustercentric radius relation (Melnick & Sargent 1977; Dressler 1980; Whitmore, Gilmore, & Jones 1993). These relations describe how the relative fraction of different morphological types varies rapidly with distance from the cluster core or with the local galaxy density. Cluster cores are dominated by elliptical and S0 galaxies whereas the outer, lower-density regions more nearly approach a spiral-rich mix of types similar to the field. It is still debated whether the dependence on density or distance from the cluster center is more fundamental. Dressler (1997) compared the morphology-density relation in local clusters with those at moderate redshift. When clusters of all types are viewed together the morphology-density relation is nearly absent at  $z = 0.5$  except for the regions of highest density where ellipticals dominate. In contrast, the low redshift sample of all cluster types shows a clear and continuous morphology-density relation. If, however, the clusters are divided into samples of high-concentration regular clusters and low-concentration or irregular clusters the situation is different. At low redshift the morphology-density relation is observed in clusters of all types whereas, at  $z = 0.5$ , only the high-concentration clusters show a clear relation. Irregular clusters show no dependence of the fractions of any particular morphological type on local density.

The Butcher-Oemler (B-O) effect (Butcher & Oemler 1984) is the third phenomenon related to cluster galaxy populations but the first to be reported. Butcher & Oemler (1984) studied a sample of 33 clusters with  $0.003 < z < 0.54$  and found a rapid increase in the fraction of blue galaxies (defined as those with B-V colors more than 0.20 mag bluer than the ridge line of early-type galaxies) with redshift. In the local Universe, the fraction of

cluster galaxies that meet this criteria is a few percent whereas, at  $z = 0.5$ , some clusters have blue fractions approaching 35% (although the redshift dependence is not uniform for all clusters). The effect continues to  $z \sim 1$  (Rakos & Schombert 1995) but there is a wide range of values even at low redshift. Lavery & McClure (1992) and Lavery & Henry (1994) found, from high-resolution ground-based imaging, that many of the Butcher-Oemler galaxies were disk galaxies with widely distributed star formation (as opposed to concentration toward the nucleus) and that galaxy-galaxy interactions appear to be responsible for the enhanced star formation in some of the systems. These effects were confirmed by HST imaging (Dressler et al 1994; Couch, Ellis, Sharples, & Smail 1994). Oemler, Dressler, & Butcher (1997) called into question a direct link between blue color and interactions and pointed out the possible effect of magnitude-selection on the spectroscopic samples.

The fourth problem of phenomenology is the role of interactions, mergers, or “galaxy harassment” (Moore et al 1996) in the evolution of cluster galaxy population. There are actually two problems. The first is the effect of interactions between galaxies and the intra-cluster medium (ICM) and the second is the effect of galaxy-galaxy interactions on the evolving population. The velocity dispersion in rich clusters is large ( $\sim 1000$  km/sec) so that galaxy-galaxy encounter velocities are typically too high for actual merging to be a probable outcome of galaxy encounters. Still there exists the possibility of modifying galaxy morphology by close encounters. Galaxy “harassment” (Moore, Lake, & Katz 1998) has been proposed as a potentially important driver of cluster galaxy evolution. Many studies note the large fraction of apparently interacting galaxies, for example Lavery & McClure (1992); Dressler et al (1994) and Couch, Ellis, Sharples, & Smail (1994). But the absence of a correlation between nearest neighbor distance and color (indicative of star formation activity) in clusters (Oemler, Dressler, & Butcher 1997) is puzzling. In contrast, van Dokkum et al. (1999) claim direct evidence in a cluster at  $z = 0.83$  for merger-driven production of massive early-type galaxies. The merger product progenitors are typically red, early-type galaxies so that they do not provide part of the solution to the B-O problem.

The most recently defined (and fifth) phenomenon to come into focus is the so-called “S0 problem”. In the study of the morphology-density relation by Dressler et al. (1997) it was found that although the fractions of galaxies of type S0 in clusters show little dependence on galaxy density either locally or at  $z = 0.5$  (regardless of cluster type), the overall fraction of the galaxy population contained in S0s is much lower ( $\sim 20\%$ ) at moderate redshift than in clusters in the local Universe (where S0s constitute  $\sim 45\%$  of the population). The spiral fraction varies in such a way to roughly balance this change with redshift. These two facts taken together suggest that some process is causing the transformation from spirals into S0s from  $z \sim 0.5$  to  $z \sim 0$ .

Our understanding of star formation in clusters—which clearly has important ramifications for all of the observational phenomena described above—has improved, to some degree, in recent years. It has been shown clearly (Balogh et al. 1997) that star formation is suppressed in clusters relative to the field and that this effect is present over the entire cluster volume out to  $\sim$  twice the virial radius. Furthermore, this effect is not due to the existence of the morphology-density relation. A comparison of cluster and field galaxies with matched sizes, and ratios of bulge-to-total luminosities (Balogh et al. 1998) shows that the cluster galaxies have distributions with lower mean star-formation rates. Large analysis of spectroscopic data to study the frequency of star-forming and post-starburst galaxies have been done by Balogh et al. (1999) and by Poggianti et al. (1999). There is real disagreement in these studies about whether post-starburst galaxies are more common in clusters relative to the field which would indicate the truncation of star-formation upon infall into the cluster. Balogh, Navarro & Morris (2000) present a modeling of the ongoing accretion of field galaxies with their star-formation declining on a gas-consumption timescale after their gas reservoirs have been stripped off by interaction with the ICM. The curious observation that the suppression of star formation occurs out to large distances from the cluster core is explained by the feature of their N-body simulations that many galaxies observed as far out as twice the virial radius have, in fact, visited the central regions of the cluster in the past.

The present study presents a large catalog of photometric and morphological measurements of a set of four X-ray luminous clusters spanning a wide range in redshift. A preliminary analysis of one of the aspects of galaxy evolution in clusters is presented.

A strong emphasis is put here on describing the fitting and analysis techniques employed, but an examination of the luminosity evolution of small disk galaxies is also presented. In §2 a description of the data selected for this study and their reduction is made, and the method used to get a quantitative description of the galaxy morphology is presented in §3. Finally, in §4 and §5 are presented and discussed the results of the study. The discussion is centered around the main result: luminosity evolution. However, other questions are raised, such as the color-magnitude and morphology-density relations, to verify the validity of the fitting technique and the reliability of the classification method applied on the galaxy sample.

All cosmology-dependent results in this paper are derived using  $H_0 = 70 \text{ km sec}^{-1} \text{ Mpc}^{-1}$ ,  $\Omega_m = 0.3$  and  $\Omega_\Lambda = 0.7$ .

## 2. DATA

### 2.1. Cluster Selection

The CNOC (Canadian Network for Observational Cosmology) cluster redshift survey (Yee, Ellingson & Carlberg 1996) is a study of 16 galaxy clusters with X-ray luminosity in excess of  $4 \times 10^{44}$  ergs s<sup>-1</sup> and with redshifts covering the range  $z = 0.2$  to  $z = 0.55$ . Such clusters are likely to be rich and virialized. The survey consists of imaging data and redshifts for approximately 2600 faint galaxies. A number of important results have been derived from this dataset, ranging from a determination of  $\Omega_m$  and  $\sigma_8$  (Carlberg et al. 1997a, 1999) to studies of evolution of galaxies (e.g. Schade et al. (1996b); Ellingson et al. (2001)).

Three clusters from the CNOC sample were chosen for further imaging with HST. They were selected out of the 16 in order to cover an interesting redshift range. They are MS1358.4+6245 (Yee et al. 1998), MS1621.5+2640 (Ellingson et al. 1997), and MS0015.9+1609 (Ellingson et al. 1998) (hereafter MS1358, MS1621, and MS0016, respectively). Existing archival imaging was supplemented with new imaging with the intent of sampling galaxies at a variety of distances from the cluster center. The cluster redshifts are presented in Table 1. In order to cover a wide range of redshifts, a fourth cluster is added to the present study, cluster MS 1054.4-0321 (MS1054) at  $z = 0.832$  (van Dokkum et al. 1999). MS1054 is also a X-ray cluster, and so has been selected on the same basis as the three CNOC clusters. MS1054 and the three CNOC clusters are part of the EMSS (*Einstein Observatory* Extended Medium-Sensitivity Survey, Gioia et al. (1990)), and their X-ray fluxes are presented in Table 1 (note, however, that a recent reanalysis of the X-ray luminosities of a cluster sample with  $0.3 < z < 0.6$  including our three CNOC clusters, suggests that the values in the EMSS are underestimated (Ellis & Jones 2002)).

The cluster galaxy sample in the present paper has an excellent redshift baseline ( $z = 0.3$  to  $z = 0.8$ ) and thus is suitable for the study of the change in galaxy properties with redshift. Secondly, it samples these clusters over a range of distance from the cluster center so that the effect of galaxy environment can be taken into account.

### 2.2. Imaging and Reduction

The original imaging of the CNOC clusters was obtained at CFHT using the multi-object spectrograph and this imaging was of moderate quality with seeing largely in the range 0.9 to 1.1 arcseconds and significant variations in the point-spread function within the frames. For the present study, additional data was acquired with the *Hubble Space Telescope*

for the three selected clusters. Clusters MS0016, MS1358, and MS1621 were observed with the WFPC2 and each field was observed with two filters: F814W and either F450W or F555W. To this data core was added previous WFPC2 observations of these clusters and of MS1054. A large quantity of data (Kelson et al. 1997) was produced for MS1358 in the F814W and F606W bands. The same filters were used to observe MS1054 (van Dokkum et al. 1999). Some additional exposures of MS0016 were taken with F814W and F555W (Proposals 8020 and 5378) <sup>3</sup>. Figure 1 shows the distribution of the galaxies in each cluster, resulting from the combination of all these data sets. The circles represent the characteristic radius of each cluster,  $r_{200}$ , the distance from the center where the average density is two hundred times the critical density of the Universe (the values of  $r_{200}$  are given in Table 1).

The data were reduced by an automated pipeline, developed at the Canadian Astronomy Data Centre, that takes as input an “association” name (defined as a group of images that can be co-added) and determines the offsets between the images (the “dither” pattern) and the other information needed to execute the stacking and sky subtraction. This pipeline is composed largely of components from a number of STSDAS <sup>4</sup> and IRAF (Tody 1993) packages. For the present study images were simply shifted and averaged. The performance of this pipeline was verified by repeating the processing for the data in this paper independently in a manual mode and inspecting the results at each stage. The output of the pipeline is the stacked and cosmic ray-rejected image. Corrections for systematic errors in the astrometry derived from the HST images using their WCS information are also made automatically by this pipeline.

A number of minor image anomalies had to be corrected before the data were analyzed. The cluster MS1358+62 was observed in the continuous viewing zone of HST (van Dokkum et al. 1998a), and most images showed large shadow stripes along the diagonals of the frame. To correct for this effect, the frames were rotated by the appropriate angle to position the stripes horizontally or vertically. Then using a long and thin median filter box, filtered images representing the shadow pattern were obtained and then subtracted from the original images. The filtered images were produced by the MEDIAN task in IRAF, which acts by replacing the central pixel of the box by the median of all the pixels in that window. The shape of the box ( $500 \times 5$  pixels) allowed the median to be computed only on the sky, leaving out the objects. After applying this correction, the sky value is more uniform, and no significant noise enhancement is noted in the previously shadowed regions. Most of the exposures also

---

<sup>3</sup>The data were retrieved through the Canadian Astronomy Data Centre, which is operated by the Herzberg Institute of Astrophysics, National Research Council of Canada

<sup>4</sup>STSDAS is a product of the Space Telescope Science Institute, which is operated by AURA for NASA

had to be corrected for bad pixels.

Photometric zeropoints in the AB system were calculated using the standard PHOTPLAM and PHOTFLAM parameters of HST imaging. The values taken are from the last updated tables<sup>5</sup>, and the zeropoints are obtained by:

$$zp = -2.5 \log(\text{photflam}) - 2.5 \log(\text{photplam}^2 / 3 \times 10^8) - 48.60$$

These magnitude zeropoints were then corrected to account for Galactic extinction with factors produced by the NASA/IPAC Extragalactic Database (NED) (values are presented in Table 1 for  $V$ -band extinction, under  $A_V$ ).

### 2.3. Galaxy Selection

A catalog of galaxies was created using the SExtractor software (Bertin & Arnouts 1996). Before doing so, the borders of the frames along the edges with insufficient signal were masked and were filled with random noise with the same dispersion as that of the actual image. This was done to avoid spurious detections that are produced by SExtractor along the edges where there is an abrupt transition from image noise to zero noise in the borders. The noise was generated using the MKNOISE task in IRAF. This procedure yields a cleaner, and no less complete, catalog of galaxies.

In order to determine the probability of detection as a function of galaxy type, simulations of the detection process were carried out. A range of galaxy types, sizes, and central surface brightness were created, convolved with the observed point-spread function, and distributed at random across the actual frames. Crowding leads to a loss of detection sensitivity and the number of galaxies simulated on each frame was limited to a reasonable number (5-10 per image) to avoid unrealistic levels of crowding. Several thousand galaxies of each type with a range of brightness were simulated for each of the clusters.

The signal-to-noise ratio at a given apparent magnitude varies from cluster to cluster and, in some cases, from image to image within a cluster. Simulations were made over all actual images of the clusters. SExtractor was run on the images that contained all of the real galaxies plus the added simulated galaxies and the list of galaxies detected by SExtractor was compared to the input list of simulated galaxies. The detection probability for a given galaxy type, size, and brightness is the ratio of number of galaxies detected to the number

---

<sup>5</sup>The tables can be found at [http://www.stsci.edu/instruments/wfpc2/Wfpc2\\_phot/wfpc2\\_photlam.html](http://www.stsci.edu/instruments/wfpc2/Wfpc2_phot/wfpc2_photlam.html)

of galaxies inserted into the images. This number is averaged over all of the fields of a given cluster.

Figure 2 shows the detection probability as percentages in the plane of observed disk central surface brightness and disk scale length in arcseconds. This figure shows the results for pure disk galaxies only. For a galaxy with a disk of a given size and surface brightness the probability of detection is increased with the addition of a bulge component. The lines on Figure 2 show the nominal limiting magnitudes ( $F814W(AB)=23.0$  for MS1054 and  $F814W(AB)=22.5$  for the other clusters) and the horizontal lines indicate the angular size that corresponds to a scale length of 2 kiloparsecs. The simulation of the detection process for disk galaxies produced the probability contours at 10%, 50%, 80%, and 95%.

Brighter than the nominal limiting magnitude the galaxy detection probability is very high (roughly 95% or better) for all disks with sizes of 2 kiloparsec or smaller. At larger sizes the samples are incomplete for low-surface brightness galaxies even though they may have integrated brightness higher than the nominal limiting magnitude. For example, in these clusters, disk galaxies with central surface brightness of  $\mu(I_{AB}) \sim 23.5$  and sizes of 0.8 arcseconds have a probability of being detected that is approximately 50%. In all of the clusters the region of large, low surface-brightness disks is sparsely populated. It is not possible to know from these data and this detection procedure whether disk galaxies are present in those regions but remain undetected or are simply not present. Therefore, we can make unbiased comparisons of the properties of the disk galaxy populations among these clusters only for scale lengths smaller than 2 kpc and at apparent brightness higher than the nominal limiting magnitude.

## 2.4. Spectroscopy and Astrometry

In order to get redshifts and other spectroscopic information from different surveys (Fisher et al. 1998; Ellingson et al. 1997; Yee et al. 1998; Ellingson et al. 1998), accurate coordinates were required for each galaxy. From the known pixel coordinates and the WCS positions of each image, approximate coordinates are calculated using the METRIC task of the STSDAS package in IRAF. This task corrects for geometric distortions specific to the WFPC2 on HST. When compared to stars that appear on the HST frames, systematic errors are frequently observed in the coordinates from the METRIC task due to errors in the HST guide star positions. To correct these errors, each frame was searched for USNO catalog (Monet et al. 2003) stars and a mean systematic offset was derived. The systematic errors should be reduced to a few tenths of an arcsecond (RMS) compared to the USNO catalog system. All the positions given in this paper are these corrected coordinates.

### 3. MORPHOLOGY

A total of  $\sim 4700$  galaxies were found by SExtractor above the initial detection threshold for each cluster ( $F814W < 24$  for MS1358 and MS1621, and  $F814W < 24.5$  for MS0016 and MS1054). Quantitative morphological measurements are made for these galaxies by fitting parametric models to the luminosity profiles (Schade et al. 1995, 1996; Marleau & Simard 1998). The use of parametric models is motivated by the fact that the galaxy profiles are of similar size to the instrumental point-spread-function and need to be corrected for this effect and for sampling. A set of commonly-accepted models is adopted here. Exponential and de Vaucouleurs profiles are used. One advantage of this quantitative approach to morphology is that a number of measurements (size, surface brightness, ratio of bulge luminosity to total luminosity) are derived from the images rather than simply a morphological class. A second advantage is that this scheme can be used to deduce evolutionary phenomena by comparing nearby and distant galaxies, if one is careful to use data that are truly comparable. Clearly, HST resolution is very valuable at  $z > 0.5$  but moderate aperture telescopes with moderate ground-based seeing can produce imaging of nearby galaxies that has similar signal-to-noise ratio at a given luminosity and similar physical resolution, in kiloparsecs, to HST. These local samples form ideal comparison datasets for HST. Further, if both the nearby and distant datasets are analyzed in a uniform manner, it is reasonable to believe that accurate evolutionary information might result from such comparisons, despite the fact that it is well-known that most galaxies show deviations, of varying degree, from the ideal models adopted here.

A disadvantage of the present approach is that comparisons with studies that are based upon visual classification (e.g. Dressler et al. (1997); van den Bergh (1990)) are difficult. For example, an intermediate galaxy might be defined (as it is here) as having a ratio of bulge-to-total luminosity  $0.4 < B/T < 0.8$ . Such a classification undoubtedly includes galaxies which would be defined as Sa, S0, and E galaxies using visual classification methods. This is a strong motivation to draw conclusions from the comparison of samples that have all been analyzed in a consistent way. Comparisons with work where visual classification is an important feature need to be done cautiously.

#### 3.1. Modeling

For a single galaxy, the images produced with both filters were fitted simultaneously. The size, ellipticity, and orientation of each component of the galaxy is assumed to be identical in both filters. The relative amplitudes of the bulge and disk components are allowed to vary independently so that the model may reproduce a galaxy whose bulge is a

different color from its disk. We chose to use the integrated color of the galaxy to accomplish the k-corrections because the individual component colors were very noisy relative to the integrated value and we present only the integrated values in the catalogs. “Postage stamp” images of the galaxies in the object catalog were produced by first measuring accurate coordinates for the center of each galaxy, and by measuring the sky value. Then, a square image centered on the new galaxy coordinates is produced and the sky is subtracted from it. The size of the box is chosen according to the fitting radius of the galaxy, which is calculated with parameters produced by SExtractor.

The first step of the fitting technique is to produce a symmetrized image, in order to eliminate strong asymmetric features or close companions. This is achieved by rotating the stamp by  $180^\circ$ , subtracting that rotated frame from the original one then clipping at  $2\sigma$  (where  $\sigma$  is the error in a given pixel accounting for sky noise and noise from the galaxy itself) of this difference image to leave only significant positive deviations from symmetry. Then this clipped image is subtracted from the original image to produce the symmetrized frame (Schade et al. 1995). A point spread function is then made, as described in Schade et al. (1996).

Symmetrized galaxies from both filter images are then fitted with three different models: a  $r^{1/4}$  bulge, an exponential disk and an hybrid model where the total luminosity is divided between a bulge and a disk components. For each model, the best fit is determined. The optimization process is done by varying the main morphological parameters: the size of the model, the axial ratio of the ellipse and its position angle, and by calculating the value of the  $\chi^2$  (Schade et al. 1995). In addition, the best fit is then submitted to a “trend test” (Sachs 1984) to look for systematic errors with radius left behind when the modeled galaxy is subtracted from the original image. This second test is necessary since the  $\chi^2$  does not account for the ordering of the pixels: it computes the distance between each pixel and the sky level as if they were all independent. Thus, a mediocre fit can yield a fairly good result at the  $\chi^2$  test. In this second test, pixels are ordered by radius from the centroid of the galaxy. The radial coordinate for this test is computed in the frame where each model is circular (in other words the ellipticity is taken into account when computing a “radial” variable for this test). Using this radially-ordered sequence, each pixel is compared with its neighbors to look for any systematic of trends. This is done by computing the mean square successive difference,  $\Delta^2$ ,

$$\Delta^2 = \sum (x_i - x_{i+1})^2 / (n - 1)$$

where  $(x_i - x_{i+1})$  is the flux difference between two successive pixels in the chain, and  $n$  is the total number of pixels. If there are no trends present, that difference is expected to be about  $2\sigma$ .

Each galaxy has then six values associated with it that will come to play in determining its type (bulge, disk, or bulge and disk) : the  $\chi^2$  and the trend statistic results for the best fit of each of the three models. Note that the values of the statistics are computed over all of the pixels in the two bands that were used in each fit.

### 3.2. Classification

#### 3.2.1. Visual Inspection

Our strategy was to use visual inspection of the fits to create a training set that would then be applied uniformly to the results of the entire fitted dataset. A large number of galaxies were examined visually together with the fitted models and the residuals of those fits. The residual images were the most helpful at assigning a type to the galaxies. This procedure also provided a subjective estimate of the effect of nearby galaxies on the fits (which should have been largely removed by the symmetrization process) and also an estimate of the frequency of failed fits. Visual inspection made it possible to estimate the magnitude, for each cluster, at which it became impossible to make a meaningful discrimination between models.

The process of deciding on class assignment (bulge, disk, or bulge-plus-disk) included access to a file of the parameters and the statistics of the fit. These played an important role in the decisions that were made. We show in Figure 3 the type of display that was used in the classification. The five images in the top row of Figure 3 are (left-to-right): the original image, the symmetrized image, the residual after the best-fit bulge has been subtracted from the original image, the residual after the best-fit disk has been subtracted and the residual after the best-fit bulge-plus-disk model has been subtracted. The numbers below the residual images are the F-test probabilities that the fit is as good as the best fit (the best fit always has a probability of 1). The 3 images in the row second from the top are the best-fit bulge, disk, and bulge-plus-disk model images. The value of the trend statistics is below those images. The 2 images on the bottom row are the bulge component of the bulge-plus-disk model and the disk component of the bulge-plus-disk model. Other information is also marked on the display. In this example the disk model is the best fit although the two component (bulge-plus-disk) model cannot be rejected at even the 5% level. It makes no difference in this case which of the two acceptable models is adopted because the fitted disk parameters are nearly identical and the bulge component is negligible, as confirmed by the images. The pure bulge model is rejected at a high level of significance.

The most obvious way to choose the best fit is to take the fit with the smallest value

of  $\chi^2$ . The reason for rejecting this approach is that the models which represent the best fit from a statistical standpoint sometimes contain components that are "un-physical" in the sense that they have components that are effectively trying to fit faint residuals of nearby neighbors that have not been fully removed by the symmetrizing process, artifacts of some kind, or even low-level errors in the sky-level estimate. This happens most frequently with bulge-plus-disk models where a legitimate (physical) component is accompanied by a second component which is unrealistic and often has very low surface brightness. A visual examination quickly identifies such components but the statistics cannot directly do so. It is important to note that our final catalog will certainly contain some errors of this type and any analysis based on the catalog needs to be sensitive to that fact.

When the quality of the fit for different models was too similar to effectively differentiate between a single component model (either bulge or disk) and the bulge-plus-disk model, the galaxy was assigned the type of the simpler model (disk or bulge). In the cases where it was impossible to visually discriminate between the bulge and the disk models, the type assigned was "uncertain". Galaxies with such type helped determine the faint magnitude limit for the sample. Initially, all galaxies with observed magnitudes (in the AB system)  $F814W < 24$  for MS1358 and MS1621, and  $F814W < 24.5$  for MS0016 and MS1054 were fitted. However, the types assigned to galaxies fainter than a magnitude of 23 are mostly "uncertain". This limit of  $F814W < 23$  corresponds exactly to that used by Dressler et al. (1997) when visually classifying galaxies from similar images.

Approximately 1100 galaxies ( $\sim 20\%$  of the data set) were inspected and classified as bulge, disk, bulge-plus-disk, or uncertain and the fit quality was recorded. The galaxies classified are a representative sample of the whole catalog, with galaxies out of each cluster and proportionally representing the whole magnitude range.

Most of the visual inspection was done by a single observer (AS), but a subset of 150 galaxies was repeated by a second observer (DS), and the two sets of classes were compared. Agreement occurred in 72% of the cases, with every disparity resulting from galaxies that fell past the faint magnitude threshold established above, or for which a single component model and the combined one were practically equivalent. There were no cases where one observer selected the bulge model when the other one preferred the disk.

### 3.2.2. *Automated Classification*

This evaluation of the fitted models for 20% of the sample was meant to produce a training set that could be used to perform an objective automated classification on the

entire sample. The goal of this process was to assign a fit type to every galaxy by comparing them to those that had been visually classified. The obvious interest of this method is to allow for a uniform classification of every galaxy, based on criteria set by the observer when the training set is built.

Galaxies were removed if they were classified by eye as “uncertain” or had fits of poor quality, for example if a nearby bright object contaminated the image. That left a training set of 415 galaxies, from all the clusters and spanning the whole range of magnitudes, although with fewer galaxies at the faint end of the distribution after the removal of the “uncertain” class.

The automated classification of the galaxies was made using the seven-dimensional space defined by the probabilities derived from the  $\chi^2$  test (3 values, one for each fit), from the trend statistics (3 values again), and by the F814W magnitude. Each galaxy was selected and assigned the same classification (bulge, disk, or hybrid) as its nearest neighbor in this parameter space. This approach was implemented because of its potential for rejecting unphysical fits. For example, it would be possible to enforce a tendency to reject very low surface brightness bulge components if a reasonable disk was already present. In fact, the nearest neighbor procedure is very general. In the end we chose not to use any of the physical parameters of the galaxies (size, surface brightness) except apparent magnitude in the automated classification.

An optimization procedure was used to determine the normalization of the axes of the parameter space which produced the largest success rate for the training set where success is defined as agreement of the automated classifier with the visually-selected class. The success rate is not sensitive to the exact values of the normalization factors and we set them to a ratio of of 2:4:1 for the  $\chi^2$ , trend statistics, and magnitude, respectively. With these values, the success rate for the computer based classification of the galaxies from the training set is 85% . The discrepancies occur for the fainter galaxies, or for the ones for which a single component model and the hybrid model were almost identical. In the former case, there will be a cut off in magnitude eliminating these uncertain classifications. In the latter, we notice that the classification process would select the combined model when the observer would prefer the single component one, but since the morphological parameters for both models are very similar in such cases, the effect is very minor.

For each cluster, a sample of the galaxies that had not been visually classified were examined to verify the automated classification procedure. No major disagreements were noticed, but the rate of error with magnitude rises significantly above F814W(AB)=23. This reinforces the faint limit of 23 established by observing at what point many galaxy types were “uncertain”. There is also an increase of the error rate at the bright end of the

distribution. This effect is caused by the large resolved structures in these luminous galaxies, which are fitted with less efficiency. However, these bright galaxies are not numerous and are not likely to be at cluster redshifts. Thus, the increase of errors at the two ends of the magnitude distribution will not significantly affect the results.

The distributions of morphological parameters in our catalogs are robust in the sense that they depend only weakly on the exact method that is used to facilitate the classification. For example, we could have used a much more direct method of choosing the best fit: accept the fit which produced the smallest value of  $\chi^2$ . If this had been done then we would have produced the same classification as our nearest-neighbor procedure for 78.4% of the training set galaxies or the same classification as our visual classes for 78.9% of the galaxies. As noted, we chose not to do this because we could produce a slightly higher success rate (85%) with the nearest-neighbor method and we could reject some, not all, "un-physical" best-fit models. The relationship between the classification procedure we used and the statistics of the fit is made more clear by examining how many real disagreements exist between the statistics of the fit and our ultimate classification. A real disagreement is produced when our classification is rejected by the F-test in favor of a classification whose fit is better from a statistical point of view. Using this definition only 2.9% of our training set galaxies represent disagreements with the statistics in the sense that our automated classification chooses a model whose fit is worse than the best-fit model at the 95% confidence level. A comparison of the visual classification and the statistics yields an identical rate of agreement. In other words, the choices made in our classification are supported by the statistics of the fits in the overwhelming majority of cases.

### 3.3. Morphological Parameters

The catalog contains a total of 1642 galaxies. Cluster MS1358 has 672 galaxies, MS1621 has 258, MS0016 has 331 and MS1054 has 381. Tables 2, 3, 4 and 5 present example of the results of the modeling and classification (the full tables are available only on-line). The name of the galaxy in column (1) contains the following information: name of the exposure, chip where the galaxy was found,  $x$  and  $y$  pixel coordinates on that chip. An asterisk put after the name indicates that the galaxy has been statistically identified as a field galaxy. Columns (2) and (3) give the coordinates of each galaxy. The observed magnitudes are given in column (4), and are the magnitudes in the reddest filter for each galaxy, F814W. Color is given in column (5) and corresponds to F814W-F555W for clusters MS0016 and MS1621, F814W-F606W for MS1054 and exposures A through I, L and M of MS1358. Exposures J and K of MS1358 are F814W-F450W. All magnitudes are in the AB system. Note that

the magnitudes are calculated from the best-fit model parameters and are thus effectively integrated to infinite radius. In the next column (except for MS1054) are presented the redshift of the galaxies for which they were available (Fisher et al. 1998; Ellingson et al. 1997; Yee et al. 1998; Ellingson et al. 1998).

The last five columns of the table present the morphologic parameters. In column (6) is  $B/T$ , which is the ratio of light in the bulge component of the galaxy and the total luminosity. If  $B/T = 0$ , the galaxy is a pure disk, and the last four columns present the properties of this disk, and if  $B/T = 1$  columns (7) through (10) list the quantitative description of this bulge. Finally, every galaxy with  $0 < B/T < 1$  is represented by two lines in the table. The first line gives its disk properties, and the second line lists the bulge parameters. In column (7),  $\mu$  is the central surface brightness, the scale length is  $H$  in (8), AR is the axial ratio (the ratio of the length of the minor axis to the major axis of the galaxy) and is presented in column (9), and the last column gives the position angle of the galaxy. The position angle is the angle between the major axis of the ellipse and the  $x$  pixel coordinate axis on the original images. The errors presented in columns (8) and (9) are mostly reliable for the single component models, and are given in the hybrid model case to indicate the average precision of the measurements.

### 3.3.1. Photometric bias and the symmetrizing process

After the fit has converged its parameters represent our best estimate of the shape of the galaxy luminosity profile. Given that shape, the normalization of the model is determined by

$$A = \frac{\sum_i \frac{O_i P_i}{\sigma_i^2}}{\sum_j \frac{P_j^2}{\sigma_j^2}}$$

where  $O_i$  is the observed counts in the  $i^{th}$  pixel and  $P_i$  and  $\sigma_i$  are the values of the model and the noise at that pixel. The normalization  $A$  is the total number of counts in the model if  $\sum_j P_j = 1$ . This relation can be derived by minimizing  $\chi^2$  under the assumption that the model is represented by the product of a shape (the  $P_j$ 's) and a normalizing factor.

As described earlier, the original image is rotated, subtracted and the difference image is clipped at  $2\sigma$  to create an asymmetric image composed of only the significant positive departures from symmetry. This image is subtracted from the original image. Statistically, there is some flux removed from the image even if it is symmetric because of the noise in the

image. The size of the effect depends on the signal-to-noise ratio and the most severe effect occurs at the background limit (that is, when background noise from sky and read-noise is the dominant noise source). Given a gaussian background noise distribution with a specific root-mean-square (r.m.s.) deviation or  $\sigma$  the clipping will leave behind 2.25% of the pixels and these will carry, on average, a signal of 0.054 times  $\sigma$  (background) for each pixel in the aperture. This signal is subtracted from the image and thus produces a bias in the measured flux. This bias is in the sense of producing less flux in the symmetric image compared to the original image.

The size of the effect depends strongly on the size of the photometric aperture and we estimate the size of the effect using values of signal and noise from our actual data for MS1358 where the galaxies are larger than in the more distant clusters. The larger size translates into larger photometric apertures and thus more background noise and a larger value of the potential bias. For the F814W (I-band) images in MS1358 we compute a bias of about 3.5% at  $I(AB) = 22$  using an aperture with a diameter of 3 arcseconds (the bias would be 6% at the limit of  $I(AB) = 22.5$  or 1.4% at  $I(AB) = 21.5$ ). However, as noted above, aperture photometry is not used to normalize our models. The approach we use optimizes the signal-to-noise ratio by weighting the pixels according to how much galaxy signal they contain. This reduces the effective number of pixels that contribute to the noise therefore it also reduces the size of the bias. For a disk galaxy at  $I(AB) = 22$  with a scale length of 0.5 arcseconds the bias is reduced by a factor of 0.57 to about 2% and for scale lengths of 0.25 and 0.10 arcseconds the bias is reduced to 0.8% and 0.2% respectively. For bulge galaxies of a given half-light radius the effect is small because the galaxies are more compact than disks. For example, at  $I(AB) = 22$  a bulge with half-light radius of 0.5 arcseconds will have a bias estimated to be 0.5%. So for typical galaxies the effect is small. Still, the existence of the bias and its variation with galaxy size is an effect to note with caution. For faint large galaxies ( $\sim 1$  arcsecond) the effect could still be 3-4%. But the effect is small in MS1358 and smaller still for our more distant clusters.

Simulations of several thousand galaxies (typically 250 galaxies per run) were done to see if we could detect any bias in the fitting of symmetrized images compared to fitting the original images. The exercise highlighted the reason that the symmetrizing process was important: fits (particularly two-component fits) to the original images are plagued with problems due to neighboring stars and galaxies. For this reason, the results that follow were computed after excluding 5-10% of the poorest fits. For disk galaxies with simulated scale lengths ( $h$ ) of 0.5 arcseconds and magnitudes of  $I(AB) = 22.5$  we recovered values of  $h = 0.52 \pm 0.15$  and  $I(AB) = 22.55 \pm 0.4$  from the original images and  $h = 0.50 \pm 0.14$  and  $I(AB) = 22.62 \pm 0.4$  from the symmetrized images. The quoted errors are the dispersions in the recovered values. At  $I(AB) = 22.5$  and  $h = 0.5$  arcseconds these galaxies have poor

signal-to-noise ratio which explains their large errors. For moderate size disks with  $h = 0.25$  arcseconds we recovered  $h = 0.27 \pm 0.09$  and  $I(AB) = 22.48 \pm 0.24$  and  $h = 0.24 \pm 0.03$  and  $I(AB) = 22.57 \pm 0.2$  from the original and symmetrized images. For very small disks ( $h = 0.10$  arcseconds) at  $I(AB) = 22.5$  we recovered values of  $h = 0.10 \pm 0.006$  and  $I(AB) = 22.54 \pm 0.06$  and  $h = 0.10 \pm 0.005$  and  $I(AB) = 22.51 \pm 0.2$  from the original and symmetrized images. Any bias due to the symmetrizing process is very small compared to the other sources of error, for example crowding by neighbors, sky subtraction, PSF uncertainty, and centering errors.

If the signal-to-noise ratios of the two images used to produce colors differ significantly from one another, it would be possible to produce a color bias from the symmetrizing procedure. This possibility was examined with the particular data from this paper and was found to be at roughly the 0.5% level when 3 arcsecond diameter apertures were used. The color bias would be smaller in our fitting procedure as noted above and is thus a negligible source of error.

The referee for this paper made the interesting suggestion that it might be possible to produce an artificial reddening of galaxies if blue star-forming regions which were distributed asymmetrically were removed by the symmetrizing process. Clearly the effect would be expected to be largest at low redshift where the regions are best resolved. The most direct way to address this issue is to perform aperture photometry (thus bypassing any dependence on the model-fitting process) on the original images and compare that photometry to the same measurements on the symmetrized images. We did this with 95 of the larger disk-dominated galaxies in the field of MS1358 without regard for whether these had been classified as cluster members or field galaxies. It was found that the offset in the mean color between the original images and the symmetrized images in MS1358 was  $0.014 \pm 0.016$  magnitudes in F814W-F606W. If a single outlier was removed then the offset became statistically significant ( $0.027 \pm 0.011$  magnitudes). If the offset were being produced by the removal of star-forming regions by the symmetrizing process then blue galaxies would be expected to show a stronger effect than red galaxies. A comparison of the blue and red halves of the sample yielded offsets of  $0.033 \pm 0.013$  and  $0.02 \pm 0.02$  magnitudes respectively. So the effect is small and is not significantly larger for the blue galaxies which should be forming stars more vigorously. A small set of large disk galaxies is available in MS1358 with F450W and F814W observations and this set should be more sensitive to the effect of star-forming regions because of the bluer filter measurement. For this set of 15 galaxies we find a reddening of  $0.003 \pm 0.07$  magnitudes ( $0.056 \pm 0.04$  if the worst outlier is removed). Again, this fails to provide support for the suggestion that the symmetrizing process is biasing the colors of galaxies by removing star-forming regions. This conclusion is supported by a visual inspection of images and symmetrized images along with the fit residuals for 50 of the larger

galaxies in both MS1358 and MS1054. There are very few cases where the effect of the symmetrizing process might plausibly produce a significant change in the structure and color of the galaxies.

### 3.3.2. *Errors on the Morphological Parameters*

The errors on single-component models (bulge or disk) are given as output from the fitting software and are generally reliable (e.g., Crampton et al. (2002)). Errors on multi-component fits suffer from the correlation of errors in the bulge and disk components which are assumed to be concentric. Because of these error correlations the errors from the fitting software may not be reliable when fitting multi-component models. Schade et al. (1999) used fits to multiple observations of the same galaxies to estimate the errors in the morphological analysis. The evaluation of the errors can be confirmed through simulations (e.g. Schade et al. (1996)). For the present paper, several hundred simulations of galaxies spanning the range of morphological parameters and signal-to-noise ratios were done. These confirm that the scatter from all sources of random error for galaxies of the size and surface brightness that this paper deals with are typically in the range of 10% in the scale length or half-light radius and 10-20% in surface brightness. The errors can be worse for large, low-surface brightness galaxies where the detection is also problematic.

## 4. RESULTS

### 4.1. Classification Reliability

#### 4.1.1. *Definition of the Morphology Classes*

The galaxy types are defined as follows: disk galaxies are taken to be the ones with  $B/T \leq 0.4$ , and bulges those for which  $B/T \geq 0.8$ . The galaxies with ratios in the range of 0.4 to 0.8 are said to be intermediate. This class is likely to include all of the S0 galaxies, as well as other bulge dominated structures that still possess a disk (early type Sa galaxies, for example). The comparison between these results and other work should therefore be done cautiously. But as will be shown in the next paragraphs, the classification still allows one to recreate classical results as accurately as a visual classification with Hubble type classes would do.

A small correction based on the individual colors of the disk and bulge components is applied to the  $B/T$  values to reduce them to rest-frame  $B$ -band.

#### 4.1.2. The Color-Magnitude Relation

One test of the reliability of these galaxy classifications is an examination of the color-magnitude relation. Bulge galaxies should be predominantly red and exhibit a tight relation. Disk-dominated galaxies would be expected to show a wider dispersion in color. Figure 4 presents the color-magnitude relations in the observed planes for the four clusters (of course some field galaxies will also be present in these fields). As expected, the distribution of colors differs between galaxies defined as bulges and those defined as later type. The bulges tend to form a tighter sequence at redder colors than the later types, which cover a wide range in color. This is especially clear for clusters MS1358 and MS1054 where the observed galaxies are concentrated in the center of the clusters (cf. Figure 1).

MS1054 shows a high concentration of faint blue disks, and an apparent gap in color between the red sequence and this group of galaxies. This suggests that there might be some galaxy groups in the field that are unrelated to MS1054 or sub-clustering in MS1054 itself to produce that bimodal distribution. It has been shown using X-ray maps produced by *ROSAT* and *CHANDRA* that there is sub-clustering in MS1054 (Donahue et al. 1998; Jeltama et al. 2001). To investigate the possibility that the bimodal distribution in the color-magnitude plane is caused by different groups being observed, the spatial distribution of the galaxies in MS1054 was examined. Looking at Figure 4, it appears that there are two distinct structures, with colors (F606W-F814W) larger and smaller than  $\sim 1$ . Figure 5 shows the spatial distribution of these two subsets on the bottom two panels, respectively. As expected, the reddest galaxies (those with (F606W-F814W)  $\leq 1.0$ ) are more concentrated towards the center of the cluster as a result of the morphology-density relation. We then expect the bluer galaxies to be distributed around that central concentration. This is what is shown in the bottom panel of Figure 5. The distribution appears uniform and not to correlate with the two clumps observed in the X-ray. The central position of these concentrations, as given in Jeltama et al. (2001), are shown on the bottom panel of Figure 5 as the open stars. The apparent presence of a concentration of blue disks north and west of the center in that plot is directly related to the spatial distribution of the observations made, as seen in Figure 1. Without redshifts to confirm the membership of these galaxies to the cluster, we will assume that we are only sampling a different population of the cluster by observing at outer radii and that these galaxies legitimately belong to the cluster. Note that a statistical correction will be made for field galaxy contamination.

### 4.1.3. *The Morphology-Radius Relation*

Another way of verifying the results of the classification, and the validity of the morphology classes, is to look at the morphology-clustercentric radius relation. It has been shown that a radial dependence of galaxy morphology inside clusters exists (Oemler 1974; Melnick & Sargent 1977). It has also been argued (Dressler 1980) that instead of projected radius, local density should be used as the independent variable, since it takes account of any sub-clustering or irregularities in the distribution of galaxies in the cluster, which was supported by the observation of a universal relation in local clusters between morphology and density. Recently, a debate has been made as to which of the two relations is more fundamental (e.g. Whitmore, Gilmore, & Jones (1993), Dressler et al. (1997), Dominguez, Muriel, & Lambas (2001)). Since we are looking at the morphology-radius only to confirm the validity of our classification, we will not present the morphology-density as well, nor try to answer that question.

The morphology-radius relation for our four clusters is presented in Figure 6. In all cases, but to various extent, the expected trends are observed: an increase in the disk population with radius, and a decrease in the number of intermediate and bulge galaxies.

## 4.2. Corrections

Rest-frame values are calculated to allow for comparison between clusters. The observed F814W(AB) magnitudes are k-corrected using the galaxy color to choose among the spectral-energy distributions (SEDs) of Coleman, Wu, & Weedman (1980). Note that AB magnitudes are used throughout. The procedure used, including the convolution of filter bands with the SEDs is described in Lilly et al. (1995). The same tables and procedures used in that work were used here. The chosen SED is then used to determine the correction from the observed wavelength to rest-frame  $B(AB)$ -band and used together with the systemic redshift of the cluster to determine rest-frame  $B(AB)$  absolute magnitude. The various colors (F814W-F606W, F814W-F555W, F814W-F450W) are transformed into rest-frame  $(U - V)(AB)$  (thereafter,  $(U - V)_0(AB)$ ) using the same SED-choosing procedure. For the galaxies that were assigned a hybrid model, k-corrections are obtained separately for the bulge and the disk from the color of each individual component. Finally, disk scale-lengths and bulge half-light radii are computed in units of kpc and surface brightnesses with restframe  $B(AB)$  magnitudes. All rest-frame values were calculated using  $H_0 = 70 \text{ km sec}^{-1} \text{ Mpc}^{-1}$ ,  $\Omega_m = 0.3$  and  $\Omega_\Lambda = 0.7$ .

#### 4.2.1. Field Galaxy Contamination

Redshifts are available for only  $\sim 15\%$  of the galaxies, so in order to have the largest sample possible, another means of defining cluster membership must be used. A statistical correction for field galaxy contamination was applied to identify probable cluster members. It should be borne in mind, however, that such a correction works only in the case where the level of actual field galaxy contamination is typical, in a statistical sense. If there were groups or clusters of galaxies in the same field as the X-ray identified clusters but at a different redshift, then this process would fail to weed them out.

To perform this correction, images of other randomly-selected fields obtained with WFPC2 were retrieved. They include 23 frames from the Groth strip and 12 frames from the *Canada-France Redshift Survey* (Lilly et al. 1995). The images were reduced, processed, and their galaxies were fitted and classified in exactly the same manner as the cluster images. For a given pair of filters, the same number of frames from the field were processed as for the cluster sample; the use of a single frame to correct all the data could introduce systematic errors. In order to avoid such errors, the subset of field galaxies used to do the correction was randomly selected and changed for each cluster frame.

It is necessary in the field correction procedure to account for the different density of sources on the frames. The field galaxies are assumed to be uniformly distributed whereas the cluster galaxies are concentrated toward the cluster center. On the scale of an individual HST pointing the distribution of galaxies appears to be clumpy rather than obeying a clear radial density gradient and this clumpiness varies from cluster to cluster. It was decided that the scale represented by a single HST pointing (there are 5 or more in each cluster) was sufficient to characterize the local density for the purpose of doing the field correction and this had the advantage of avoiding the assumption of a very regular galaxy distribution which is only true in an average sense. Each pointing was corrected individually.

The randomly selected galaxies for a given field were “matched” with the cluster galaxies. The cluster galaxy that most closely resembles each field galaxy is marked as a “statistically identified field galaxy” and removed from the cluster sample. The parameters used to do that matching are the observed magnitude, the color, and the  $B/T$  ratio. The best match was defined using the same type of procedure as applied for the classification. A space was constructed and the nearest neighbor of each field galaxy in the cluster was removed. Clusters MS1358, MS1621 and MS0016 were corrected up to a magnitude of  $F814W(AB) = 22.5$ , and MS1054 up to  $F814W(AB) = 23.0$ .

The color-magnitude relation is used in Figure 7 to illustrate the effect of the field galaxy contamination correction. The red bulge sequence is relatively un-modified and many of the

galaxies off the sequence are identified statistically as interlopers from the field. For MS1358, there was a large number of galaxies redder than the reddest ellipticals in the core of the cluster, which were believed to be either higher redshift background galaxies or very dusty foreground galaxies. The correction identifies most of them as field galaxies. In MS1054, as discussed in §4.1.2, there are two groups visible in the color-magnitude diagram, one which lies in the bluer region of the plot (c.f. Fig. 4). That “blue group” of galaxies is largely removed by the statistical correction process.

Another means of verifying the results of the field galaxy correction is to compare the sample of field galaxies used to do the correction to the ones rejected from the cluster frames. This comparison is done using one of the parameters that remained free during the matching process: the disk scale length. The distribution of the sizes from the two samples were compared using a Kolmogoroff-Smirnoff test with the result that the hypothesis that the two samples of scale lengths are drawn from the same distribution cannot be rejected at the 5% level (the K-S probability was 7%). This indicates that the galaxies in the cluster field that are designated as field galaxies are similar to the field galaxies used to do the corrections. We have forced them to be similar in terms of color, magnitude, and bulge-to-total luminosity and, after doing so, we find that the scale length distributions are not distinguishable.

#### 4.2.2. *Normalization by Mass*

It is impossible to do a reasonable comparison of the number counts of galaxies between the four clusters directly because the clusters vary in mass and because the completeness and the radial coverage of the sampling varies enormously from cluster to cluster (as shown in Figure 1). In order to correct for this problem, a normalization factor was computed based on the fraction of cluster mass that was sampled by the fields observed in the present study. The calculations take into account the mass of each cluster, the field of view, and the density profile of the clusters, and are made under the assumption that the cluster mass is a good predictor of the total number of galaxies it contains. In other words, we are assuming that the efficiency of galaxy formation is identical in these four clusters. Further, we implicitly assume that the efficiency of production of each galaxy type is constant across clusters.

In a study based on the CNOC clusters, Carlberg et al. (1997b) have shown that the galaxy number density profile is proportional to the cluster mass profile, at least over a given range in radius ( $0.1 \leq r/r_{200} \leq 1.5$ ). Therefore, by selecting an appropriate density profile and integrating it over the field of view, a good estimate of the mass that has been sampled can be made. This can be converted into an expected number of galaxies under

the assumptions stated above. In the study by Carlberg et al. (1997b), it is shown that the function  $\rho(r) \propto r^{-1}(r + a_\nu)^{-2}$  is adequate to describe the mass distribution of 14 of the 16 CNOC clusters, including the three studied here (this model is similar to the one presented by Navarro, Frenk, & White (1995)). Therefore, it will be used to represent the three-dimensional spatial density profile of the clusters, with a value for the scale radius,  $a_\nu$ , of 0.27 as suggested by the best fits of Carlberg et al. (1997b).

To compute the normalization factor, the assumption that the clusters are spheres containing their galaxies within  $r = 1.5r_{200}$  is made. First,  $\rho(r)$  was integrated to project it in the plane. This produces  $\phi(r)$ , the surface density which is then normalized by the integral of  $\rho(r)$  over the whole sphere. This normalized surface density is then integrated over the entire field of view of the observations. The fraction of the cluster observed is then known, and multiplying it by the cluster mass (as presented in Table 1) gives the normalization factor that we seek.

The results are sensitive to the cluster masses. Estimates of the mass of MS1054 have been made using various techniques: X-ray luminosity (Donahue et al. 1998; Jeltama et al. 2001), weak lensing (Hoekstra, Franx, & Kuijken 2000), and observed velocity dispersion (Tran et al. 1999). The value calculated with this last technique is the one adopted here, since it is very similar to that used to evaluate the masses of the CNOC clusters (Carlberg et al. 1996). The values of the normalization factor are presented in Table 6.

### 4.3. Disk Galaxy Surface Brightness Distributions

In this section, the distribution of disk surface brightnesses is investigated in the four clusters. It is important to note that these galaxies are identified as “disk” galaxies solely on the basis of the light profiles, in the sense that exponential profiles provide better representations of their luminosity distributions than are provided by de Vaucouleurs profiles.

#### 4.3.1. Magnitude Selection

Figure 8 shows the relationship between the scale length and the rest-frame B-band central surface brightness of the disks in those galaxies with  $B/T \leq 0.4$  and with magnitudes brighter than  $F814W(AB)=22.5$  (23.0 for MS1054). At each cluster redshift, the cutoff in observed magnitude translates into a cutoff in luminosity (modified slightly by variation of the K-correction with color). Disk central surface brightness ( $\mu_{0disk}$ ) depends on both disk

scale length ( $h_{kpc}$ ) and absolute B magnitude ( $M_{Bdisk}$ ) as :

$$\mu_{0disk} = M_{Bdisk} + 2.5 \log(2\pi) + 5 \log(h_{kpc}) + 36.565$$

The dotted lines represent these limiting luminosities in terms of size and surface brightness. Figure 8 also indicates on each frame the magnitude cutoff for MS1054.

The analysis of the sensitivity of our source detection procedure to disk galaxies shows that the probability of detecting pure disk galaxies in all of the clusters is high ( $> 95\%$ ) brighter than the nominal limiting magnitudes only for those galaxies with scale lengths smaller than 2.0 kiloparsecs in all clusters. Therefore the region of the diagrams shown in Figure 8 to the left of the magnitude selection lines and with scale lengths smaller than 2.0 kpc is fairly sampled in all of the clusters. That is, fair comparisons of the size-surface brightness distributions can be made only in this region. In practice we limit our consideration to disk galaxies with  $h < 2$  kpc. The most striking feature of Figure 8 is the increase with redshift in the number of small ( $h < 2$  kpc), high surface brightness disk galaxies. This effect could be produced in a number of ways. This could be an actual evolutionary effect. Or it could be that the populations of disk galaxies in all of the clusters are similar but that the sampling rate of the population in MS1054 is much higher than in the other clusters so that the observed number is larger although the underlying distributions are identical. If the clusters do not represent a family with a common evolutionary history then the difference in the number of small disk galaxies may not be an evolutionary effect but merely an indication of the range of characteristics of the galaxy populations in rich clusters.

In the next section, an attempt will be made to address the issue of the different sampling rates in the four clusters by normalizing the counts on the basis of the sampled mass in each observation. This will be based on the conjecture that disk galaxy formation is equally efficient in all of these clusters. Another way of saying this is that a given quantity of total mass (dark plus baryonic) will produce a given quantity of disk galaxy mass. The uncertainty of this conjecture is obvious and the fact that the disk galaxy populations may be in different phases of their evolution in different clusters is a further caveat.

Nevertheless, we will proceed to investigate the difference in the properties of these galaxies under the assumptions that we have stated above. The simplest pair of models to describe the change in the size-surface brightness distribution is a) a shift in size of the entire distribution with no change in surface brightness, and b) a shift in surface brightness of the population with no change in size.

#### 4.3.2. *Pure Disk Size Evolution*

Pure size evolution of disk galaxies (by definition with no change in surface brightness) is a way to model changes in the statistical distributions that are observed in these samples. But this model is difficult to link in a simple way to a physical scenario for the evolution of individual galaxies because some change in star formation rate is likely to occur over time and passive evolution of the stellar population will change the disk surface brightness even if the star formation rate is maintained at some constant level. It is conceivable that a changing star-formation rate could balance an aging population that is fading but it seems unlikely because it would require an interesting degree of fine-tuning if it were to be observed over a population of galaxies.

In general, evolving disks are expected to grow in size as they add more mass (e.g., Mao, Mo, & White (1998)). In the present case we observe many small galaxies at a given central surface brightness in MS1054 at  $z = 0.83$  which are absent in the lower redshift clusters. The way for them to escape detection in these lower redshift clusters is for them to evolve to smaller sizes (at a given surface brightness) as time moves forward. This is directly contrary to a simple model of disk growth. Therefore, we have reason to be skeptical of the pure size evolution as a physical model for evolution for individual galaxies. Nevertheless, we will test pure size evolution as a model for the evolution of the distributions of size and central surface brightness.

To do this test, the size distribution of each cluster is shifted (in size only) until the “equivalent expected number” of galaxies above the selection line is the same as the observations of MS1054. This means that the ratio of observed numbers of galaxies above the selection line is equal to the ratio of the normalizing factors which correct for cluster mass and the spatial coverage of the observations, as calculated in §4.2.2 (the “equivalent expected number” for each cluster is given in column 2 of Table 7). In other words, the whole galaxy sample for a given cluster is shifted in size until the expected number of galaxies appears in the region of the size-surface brightness plane where the small bright disks are found. This region is the one represented in Figure 8. The shifts in the disk scale length distributions required are given in the third column of Table 7.

A problem with this test appears immediately: a shift in size is unable to provide the expected number of small bright disks for MS1358 and MS0016. We can only shift the distributions in size until the selection line due to limiting magnitude in each cluster coincides with the corresponding selection line in MS1054. Beyond this shift we have no sensitivity to smaller galaxies in MS1358, MS1621, and MS0016. The shift given in Table 7 is the shift that gives the largest number of small bright disks and is roughly the largest shift we can do for MS1358 and MS0016. This problem is not due to the poorer sampling

of these clusters since the normalization technique used to calculate the expected numbers removes the effects of the different areas sampled. The shifted distributions are plotted in Figure 9. In that plot, the lines are the same as in Figure 8, i.e., the magnitude cutoff of MS1054 and the 2 kpc scale length cut off.

#### 4.3.3. *Pure Disk Surface Brightness Evolution*

The limiting size at which detection of disk galaxies is complete varies from cluster to cluster as given above. At this limiting size there is a limiting central surface brightness imposed by the magnitude limit. The region of the size-surface brightness plane that is complete for all of the clusters has a limiting size of 2.0 kpc and at this scale length each cluster has its own limiting surface brightness. For MS1358, MS1621, MS0016, and MS1054 this limiting surface brightness is roughly 22.6, 21.8, 21.1, and 20.3 respectively. Thus we can shift each cluster population by, at most, the difference between its limiting surface brightness at 2 kpc and that of MS1054. If we shift it more than this amount then we are no longer comparing complete regions of the size-surface brightness plane.

The simplest model that is suggested by these data is a uniform change in surface brightness experienced by the entire disk galaxy population. To test this model the population is shifted in surface brightness only, subject to the constraint above, namely, that we are careful to compare only well-sampled regions of the size-surface brightness plane. The shift produces an acceptable model when the observed number in the well-sampled region of the clusters agree with the expected number of galaxies predicted from the MS1054 data using the mass normalization to account for cluster mass and variation of our sampling. The results are shown in Figure 10. The 95% confidence intervals for these shifts were estimated using procedures described by Gehrels (1986).

The number of disks in the region where they can confidently be compared (scale length smaller than 2 kpc and surface brightness high enough to be detected in MS1054) is different in MS1358 and MS1054 at greater than the 99.9% confidence level. The galaxy populations differ by more than the difference in sampled mass would indicate. The shifts that are required in order to bring the number of observed galaxies in our comparison region into line with the number predicted by the mass normalization factor (together with the number in MS1054) are given in Table 7. At the 95% confidence level only MS1358 differs, to a degree that is statistically significant, from MS1054 although the best-fit shifts in surface brightness are always non-zero.

The comparison of MS1358 and MS1054 indicates that a shift of  $1.50^{+0.26}_{-0.80}$  magnitudes

(95% confidence level) in surface brightness produces agreement in the number of small disks and, furthermore, the median scale lengths and dispersion in the resultant samples agree reasonably well (the values are shown in Table 7). The statistics for the other clusters are poor because of small numbers of galaxies.

A simple model such as pure evolution of the disk population in surface brightness is unlikely to provide a complete explanation of the observations. Nevertheless, with the statistics in hand on these four clusters, such a model explains the main features of the size-surface brightness distributions of small disks in these four clusters. In particular, it models the discrepancy in the small disk population between MS1358 at  $z = 0.3$  and MS1054 at  $z = 0.83$ .

Another way of estimating the apparent change in surface brightness of these galaxy populations is by visual examination of the upper-left envelope to the distribution in the plane of size and surface brightness. This envelope, where the maximum scale length at a given surface brightness increases with fainter surface brightness may be explained by the higher angular momentum of low surface brightness galaxies, which results in larger disk sizes for a given mass (Dalcanton, Spergel, & Summers 1997). Since the existence of this envelope is, plausibly, an intrinsic physical property of the galaxies, tracking it through the different clusters allows one to get an estimate of the luminosity evolution of the galaxies. On Figure 11 are traced both the limiting magnitude of each cluster and the estimated position of the upper envelope, represented by constant magnitude lines on each frame. Both upper and lower limits for this upper envelope are plotted. This time, the  $\Delta\mu_0$  represent the shift between the upper envelope of each cluster and the one of MS1054. The shifts are simply estimated by eye. The values are given in the last column of Table 7. The ranges just overlap with those previously calculated in the cases of MS0016 and MS1621, but are somewhat smaller for MS1358. There is reasonable agreement of this result with the previous estimation of the surface-brightness evolution that used a more rigorous statistical procedure.

In summary, a simple model of the change in the distribution of small disk properties in the plane of size and surface brightness is pure surface-brightness evolution. If interpreted physically this implies a brightening of  $\sim 1.5$  magnitudes in the B band over the range  $z = 0.3$  to  $z = 0.8$ .

#### 4.3.4. *Can we discriminate between disks and bulges at small sizes?*

The results of the preceding sections raises the question of whether we could be making the error of classifying galaxies as disks when they are actually bulges. The frequency of

such errors might vary with redshift producing a spurious population of small disk galaxies at high redshift. In Figure 12 we show that we can distinguish reliably between disk and bulge models even for very small and faint galaxies in the field of MS1054.

In order to quantify our success rates at distinguishing bulges and disks we simulated galaxies including all sources of error and subjected them to the end-to-end fitting and classification process. Note that the fits to actual data were done by simultaneously fitting the images in two filters whereas these simulations were done using only a single image. The magnitude scales were accurate so that the signal-to-noise was reproduced exactly for the I-band images in the simulations. This means that our simulations actually had lower signal-to-noise ratios than the two-filter fits that were used for the real data. Therefore, these simulations produce results that are lower quality than our actual fits. This simplified the simulation procedures and is sufficient to illustrate the effectiveness of the fitting process.

The resolution in physical units is lowest in MS1054. Simulations were done of 800 disks with a scale length of 0.10 arcseconds and these galaxies were added to actual MS1054 images in order to include the effects of neighbors and crowding. The galaxies went through the same detection and symmetrizing processes as the real data. Uncertainties in the point-spread function and sky level were effectively included. The fits were processed through the automated classification procedure.

Pure disk galaxy models with true (simulated) scale lengths of 0.1 arcseconds and  $I(AB) = 22.5$  were classified as pure disks in 90.2% of the cases. In 91.8% of the cases the disk parameters were recovered effectively with the galaxy classified as either pure disk or bulge-plus-disk. In the latter case this implies a negligible bulge component although the class chosen was bulge-plus-disk. In 3.4% of the cases the simulated disks were classified as pure bulges. In the remaining 4.8% of the cases the fits failed to converge to a reasonable result.

The mis-classification as disks of galaxies that are actually bulges is a serious concern. We simulated and fit approximately 800 pure bulge galaxies with half-light radii  $R_e = 0.167$  arcseconds and  $I(AB) = 22.5$ . This corresponds to the same half-light radius as a pure disk with scale length of 0.1 arcseconds. We claim success (recovery as a pure bulge in 73% of the cases or recovery as a bulge-dominated bulge-plus-disk galaxy where the bulge parameters were well-determined in 23.9% of the cases) in a 96.9% of the cases. Our end-to-end simulations mistakenly classified a pure bulge as a disk in 1.3% of the cases. The remaining 1.8% were fits which failed to converge.

These simulations also yield estimates of the errors on our fitted parameters by comparing the distributions of recovered parameter values to the known input values. The errors do

not decrease rapidly with increasing signal- to-noise ratio indicating that they are dominated by small systematic errors such as errors in the point-spread function, sky level estimate, galaxy centering, and other details of the processing procedure. For the smallest galaxies (half-light radius  $\sim 0.2$  arcseconds) at  $I(AB) = 22.5$  the dispersion in both recovered size and magnitude hover around 10% and grow to about 15% as the size doubles at a fixed luminosity. As the half-light radius approaches 1 arcsecond the dispersion in recovered size approaches 30% and the error in brightness is about 0.35 magnitudes. There are not many galaxies this large in the catalog. Systematic errors are seen as failures of the mean recovered values to converge on the true value even for large sample sizes but these systematics are always less than the dispersions and the worst cases are for small galaxies where the systematics can be 50-60% as large as the random errors. For the majority of galaxies in our catalog the total errors in size and brightness parameters are in the range of 10% for smaller galaxies and 20% or less for most of the catalog galaxies.

In summary, these results indicate that we can reliably distinguish between bulges and disks near the magnitude limit of our observations and at very small galaxy sizes where the interesting results of our study fall.

## 5. DISCUSSION

The cluster MS1054 apparently contains a population of small, high-surface brightness disk-like galaxies that are not seen in the other three clusters at lower redshift. These galaxies are referred to as “disks” because they are better fit by an exponential profile than by a de Vaucouleurs  $r^{1/4}$  law. These galaxies are reminiscent of the high-surface brightness field “disk” populations detected by Schade et al. (1995, 1996), and Guzmán et al (1996). Under the assumption that the observed differences in the small disk-galaxy populations in these four clusters are due to evolution, then pure surface brightness evolution describes the observations somewhat better than pure size evolution. Neither model is perfect and our ability to distinguish between them is limited by the small numbers of galaxies involved in the comparison. More complex models have not been investigated.

Using two independent techniques, the luminosity enhancement of the disk galaxies was estimated. The method based on the detection of the upper limit of the distribution of galaxies in the size-surface brightness plane is free of any assumptions on the mass and population of the cluster. It provides a range of values for the shift in surface brightness observed in the galaxy population from cluster to cluster. The other technique, based on the cluster mass normalization factors, gives another estimate for each cluster.

The agreement between the results of the two techniques is encouraging in terms of the validity of the counts normalization method. To further test it, larger samples would be required such that statistics could be made with larger number. As it was seen with these clusters, the larger the data set, the easier it is to get accurate results when trying to find the “equivalent expected number” of galaxies, as done in section 4.3. One must also keep in mind the assumptions that were made, mainly that the number of disks observed in a cluster is directly proportional to the total mass of the cluster, and that the galaxy number density profile is proportional to the mass profile. Even though this second assumption is supported by previous work (Carlberg et al. 1997b), the first one albeit reasonable has yet to be proven.

Because of all the assumptions made, the result on the luminosity evolution of the galaxies needs to be considered carefully, in the context of previous work. Schade et al. (1996c) have shown that disk galaxies, both in the field and in clusters, have a mean surface brightness increased by  $\sim 1$  magnitude at  $z = 0.55$  compared to local clusters. Similar conclusions have also been reached in other works (e.g. Forbes et al. (1996); Roche et al. (1998)). Maller-Ornelas et al (1999) studied the population of small bright disks and showed that this rapidly-evolving population has sizes and velocity widths typical of irregular galaxies in the local Universe but are typically  $\sim 2$  magnitudes more luminous than local irregulars.

The most obvious caveat accompanying our conclusions about the evolution of small disk galaxies is that the cluster membership of these galaxies is uncertain. Redshifts are not available for all galaxies. Corrections for field galaxy contamination have been made but these corrections apply only to typical fields and it may be that there are atypical levels of contamination by non-cluster members. In other words, we may be seeing an effect that is not only unrelated to the cluster environment but is erroneous because the cluster redshifts have been assumed for all cluster “members” and these redshifts would be incorrect if membership were incorrectly assigned. Redshifts would make these conclusions far more secure.

To further rule out the possibility that the small bright disks observed in MS1054 are contaminants, their spatial distribution is observed. The small bright disks are not concentrated in any region of the cluster, as evidenced by Figure 13, such as it would be expected if they were members of a group projected in the field of MS1054, or of a subgroup falling into the cluster. The small bright disks of all clusters were visually examined. They all appear to form one population of compact and regular disks. The fact that these galaxies are observed in all clusters, even though there are many more in MS1054, is another argument to assume that they are not observed in MS1054 because of a field-of-view contamination.

## 6. SUMMARY AND CONCLUSION

A catalog of  $\sim 1600$  galaxies from the rich clusters MS0016, MS1054, MS1358, and MS1621 is presented. It shows positions, photometry, and quantitative morphology obtained through modeling of the galaxies. Each galaxy was fitted with three different models (bulge, disk, bulge and disk), and assigned a type based on the comparison of the best fit of each model (as evaluated by the  $\chi^2$  optimization). The galaxies were then classified by both an observer for a subset, and by a computer script for all the data set. The classification produces the morphology measurements: the bulge-to-total luminosity ratio, the scale-lengths, axial ratios, position angles and surface brightnesses of both the bulge and disk components of the galaxies.

The validity of these techniques was tested by comparing the results they produce to well known properties of cluster galaxies. First of all, the color-magnitude relation made with observed values is examined. The galaxies assigned a “bulge” type are concentrated in the region of the red sequence, a tight distribution in the color-magnitude plane. This is in agreement with the known fact that the red sequence is formed by the ellipticals in the center of the cluster. The disk galaxies generally have bluer colors, and the scatter increases with fainter magnitudes. Secondly, the morphology gradients observed in the clusters through the morphology-radius relation with the morphology classes defined in this paper are those expected: the number of disk galaxies increases with radius, while the intermediate and bulge galaxies are more numerous in the inner regions of the cluster.

The catalog of measurements was applied to the study of luminosity evolution of disk galaxies. A population of small ( $h < 2\text{kpc}$ ), high surface brightness disks is observed in MS1054. Some of these disks are also present in the other clusters, but in much smaller numbers. Two models were tested to account for the presence of the small bright disks in MS1054: the first model considers a size evolution with redshift, and the second a luminosity evolution. The size evolution model is not successful at describing the data. The luminosity evolution model does a good job, albeit not perfect, at explaining the differences in population with redshift. As a result, a luminosity enhancement of  $\sim 1.5$  magnitude from  $z = 0.3$  to  $z = 0.8$  was observed.

## REFERENCES

- Balogh, M.L., Navarro, J.F., & Morris, S.L. 2000, *ApJ*, 540, 113
- Balogh, M.L., Morris, S.L., Yee, H.K.C., Carlberg, R.G., & Ellingson, E. 1999, *ApJ*, 527, 54

- Balogh, M.L., Schade, D., Morris, S.L., Yee, H.K.C., Carlberg, R.G., & Ellingson, E. 1998, *ApJ*, 504, L75
- Balogh, M.L., Morris, S.L., Yee, H.K.C., Carlberg, R.G., & Ellingson, E. 1997, *ApJ*, 488, L75
- Bertin, E. & Arnouts, S. 1996, *A&A*, 117, 393
- Bower, R., Lucey, J., & Ellis, R. 1992 *MNRAS*, 254, 601 D., Davies, R. L., Faber, S. M., Terlevich, R. J., & Wegner, G. 1987, *ApJ*, 313, 42
- Butcher, H. & Oemler, A., Jr. 1984, *ApJ*, 285, 426
- Carlberg, R., Yee, H., Morris, S., Lin, H., Ellingson, E., Patton, D., Sawicki, M., & Shepherd, C. 1999, *ApJ*, 516, 552
- Carlberg, R. G., Morris S. L., Yee, H. K. C., & Ellingson, E. 1997, *ApJ*, 479, 19
- Carlberg, R. G., Yee, H. K. C., Ellingson, E., Morris, S., Abraham, R., Grabel, P., Pritchet, C. J., Smecker-Hane, T., Hartwick, F. D. A., Hesser, J. E., Hutchings, J. B., & Oke, J. B. 1997, *ApJ*, 485, L13
- Carlberg, R. G., Yee, H. K. C., & Ellingson, E. 1997, *ApJ*, 478, 462
- Carlberg, R. G., Yee, H. K. C., Ellingson, E., Abraham, R. G., Gravel, P., Morris, S., & Pritchet, C. J. 1996, *ApJ*, 462, 32
- Coleman, G. D., Wu C.-C., Weedman, D. W. 1980, *ApJS*, 43, 393
- Couch, W., Ellis, R., Sharples, R., & Smail, I. 1994, *ApJ*, 430, 121
- Crampton, D., Schade, D., Hammer, F., Matzkin, A., Lilly, S. J., & Le Fèvre, O. 2002, *ApJ*, 570, 86
- Dalcanton, J. J., Spergel, D. N., & Summers, F. J. 1997, *ApJ*, 482, 659
- Djorgovski, S., & Davis, M. 1987 *ApJ*, 313, 59
- Donahue, M., Voit, G. M., Gioia, I., Luppino, G., Hughes, J. P., & Stocke, J. T. 1998, *ApJ*, 502, 550
- Dominguez, M., Muriel, Hernan, & Lambas D. G. 2001, *ApJ*, 121, 1266
- Mallen-Ornelas, G., Lilly, S., Crampton, D., & Schade, D. 1999 *ApJ*, 518, 83

- Dressler, A. 1980, *ApJ*, 236, 351
- Dressler, A. 1984, *ARA&A*, 22, 185
- Dressler, A., Lynden-Bell, D., Burstein, D., Davies, R. L., Faber, S. M., Terlevich, R. J., & Wegner, G. 1987, *ApJ*, 313, 42
- Dressler, A., Oemler, A., Butcher, H. & Gunn, J. 1994 *ApJ*, 430, 107
- Dressler, A., Oemler, A. Jr., Couch, W. J., Smail, I., Ellis, R. S., Barger, A., Butcher, H., Poggianti, B. M., & Sharples, R. M. 1997, *ApJ*, 490, 577
- Ellingson, E., Yee, H. K. C., Abraham, R. G., Morris, S. L., Carlberg, R. G., & Smecker-Hane, T. A. 1997, *ApJS*, 113, 1
- Ellingson, E., Yee, H. K. C., Abraham, R. G., Morris, S. L., & Carlberg, R. G. 1998, *ApJS*, 116, 247
- Ellingson, E., Lin, H., Yee, H. K. C., & Carlberg, R. G. 2001, *ApJ*, 547, 609
- Ellis, S. C., & Jones, L. R. 2002, *MNRAS*, 330, 631
- Ellis, R. S., Smail, I., Dressler, A., Couch, W. J., Oemler, A. Jr., Butcher, H., & Sharples, R. M. 1997, *ApJ*, 483, 582
- Fisher, D., Fabricant, D., Franx, M., & van Dokkum, P. G. 1998, *ApJ*, 498, 195
- Forbes, D. A., Phillips, A. C., Koo, D. C., & Illingworth, G. D. 1996, *ApJ*, 462, 89
- Gehrels, N. 1986 *ApJ*, 303, 336
- Gioia, I. M., Maccacaro, T., Schild, R. E., Wolter, A., Stocke, J. T., Morris, S. L., & Henry, J. P. 1990, *ApJS*, 72, 567
- Gladders, M. D., Yee, H. K. C., & Ellingson, E. 2002, *AJ*, 123, 1
- Guzman, R., Koo, D., Faber, S., Illingworth, G., Takamiya, M., Kron, R., & Bershadsky, M. 1996 *ApJ*, 460, 5
- Hoekstra, H., Franx, M., & Kuijken, K. 2000, *ApJ*, 532, 88
- Hubble, E. & Humason, M. L. 1931, *ApJ*, 74, 43
- Jeltema, T. E., Canizares, C. R., Bautz, M. W., Malm, M. R., Donahue, M., Garmire, G. P. 2001, *ApJ*, 562, 124

- Kelson, D. D., van Dokkum, P. g., Franx, M., Illingworth, G. D., & Fabricant, D. 1997, *ApJ*, 478, L13
- Lavery, R. Pierce, M., & McClure, R. 1992 *AJ*, 104, 2067
- Lavery, R. & Henry, J. 1994 *ApJ*, 426, L524
- Lilly, S. J., Le Fevre, O., Crampton, D., Hammer, F., & Tresse, L. 1995, *ApJ*, 455, 50
- Oemler, A. Jr. 1974, *ApJ*, 194, 1
- Oemler, A., Dressler, A., & Butcher, H. 1997 *ApJ*, 474, 561
- Mao, S., Mo, H. J., & White, S. D. M. 1998, *MNRAS*, 297, L71
- Marleau, F. R., & Simard, L. 1998, *ApJ*, 507, 585
- Martel, H., Premadi, P., & Matzner, R. 1998, *ApJ*, 497, 512
- Melnick, J. & Sargent, W. L. W. 1977, *ApJ*, 215, 401
- Monet, D.G., et al. 2003, *AJ*, 125, 984
- Moore, B., Katz, N., Lake, G., Dressler, A., Oemler, A. Jr. 1996 *Nature*, 379, 613
- Moore, B., Lake, G., & Katz, N. 1998 *ApJ*, 495, 139
- Navarro, J. F., Frenk, C. S., & White, S. D. M. 1995, *MNRAS*, 275, 720
- Poggianti, B.M., Smail, I., Dressler, A., Couch, W.J., Barger, A.J., Butcher, H., Ellis, R.S., & Oemler, A.J. 1999, *ApJ*, 518, 576
- Rakos, J. & Schombert, J. 1995 *ApJ*, 439, 47
- Roche, N., Ratnatunga, K., Griffiths, R. E., Im, M., & Naim, A. 1998, *MNRAS*, 293, 157
- Rosati, P., della Ceca, R., Norman, C., Giacconi, R. 1998 *ApJ*, 492, L21
- Sachs, L. 1984, *Applied Statistics*. Second edition, Springer-Verlag, New York, 373
- Schade, D., Lilly, S. J., Crampton, D., Hammer, F., Le Fèvre, O., & Tresse, L. 1995, *ApJ*, 451, L1
- Schade, D., Lilly, S. J., Le Fèvre, O., Hammer, F., & Crampton, D. 1996, *ApJ*, 464, 79
- Schade, D., Carlberg, R., Yee, H., Lopèz-Cruz, O. & Ellingson, E. 1996, *ApJ*, 464, 163

- Schade, D., Carlberg, R. G., Yee, H. K. C., & Lopèz-Cruz, O. 1996, ApJ, 465, L103
- Schade, D., Barrientos, L. F., & Lopèz-Cruz, O. 1997, ApJ, 477, L17
- Schade, D., et al. 1999, ApJ, 525, 31
- Tody, D. 1993, "IRAF in the Nineties" in *Astronomical Data Analysis Software and Systems II*, A.S.P. Conference Ser., Vol 52, eds. R.J. Hanisch, R.J.V. Brissenden, & J. Barnes, 173
- Tran, K. H., Kelson, D. D., van Dokkum, P., Franx, M., Illingworth, G. D., & Magee, D. 1999, ApJ, 522, 39
- van den Bergh, S. 1990, ApJ, 348, 57
- van Dokkum, P. G., Franx, M., Kelson, D. D., Illingworth, G. D., Fisher, D., & Fabricant, D. 1998, ApJ, 500, 714
- van Dokkum, P. G., Franx, M., Kelson, D. D., & Illingworth, G. D. 1998, ApJ, 504, L17
- van Dokkum, P. G., Franx, M., Fabricant, D., Kelson, D. D., Illingworth, G. D. 1999 ApJ, 520, L95
- van Dokkum, P. G., Franx, M., Fabricant, D., Illingworth, G. D., Kelson, D. D. 2000, ApJ, 541, 95
- Whitmore, B. C., Gilmore, D. M., & Jones, C. 1993, ApJ, 407, 489
- Yee, H. K. C., Ellingson, E., & Carlberg, R. G. 1996 ApJS, 102, 269
- Yee, H. K. C., Ellingson, E., Morris, S. L., & Carlberg, R. G. 1998, ApJS, 116, 211

Table 1. Cluster properties

Cluster	$\alpha_{2000}$	$\delta_{2000}$	z	$L_X(0.3\text{-}3.5\text{ keV})$ ( $10^{-13}\text{ erg cm}^{-2}\text{s}^{-1}$ )	Mass ( $10^{15} M_\odot$ )	$r_{200}$ arcsec	$\sigma$ km s $^{-1}$	$A_V$ mag
MS 1358+62	13:59:50.69	62:31:05.44	0.3290	13.82	2.15	411	937	0.075
MS 1621+26	16:25:38.36	26:27:42.59	0.4275	9.74	1.52	278	793	0.106
MS 0016+16	0:21:09.01	16:42:54.54	0.5479	7.98	2.59	353	1234	0.182
MS 1054-03	10:56:59.94	-3:37:36.48	0.832	2.62	3.50	239	1170	0.117

References. — column (4) Yee, Ellingson & Carlberg (1996), and van Dokkum et al. (2000) for MS1054; column (5) Gioia et al. (1990); column (7) Carlberg, Yee, & Ellingson (1997) and Tran et al. (1999) for MS1054; columns (6 and 8) Carlberg et al. (1996), and Tran et al. (1999) for MS1054; column (9) NASA/IPAC Extragalactic Database (NED)

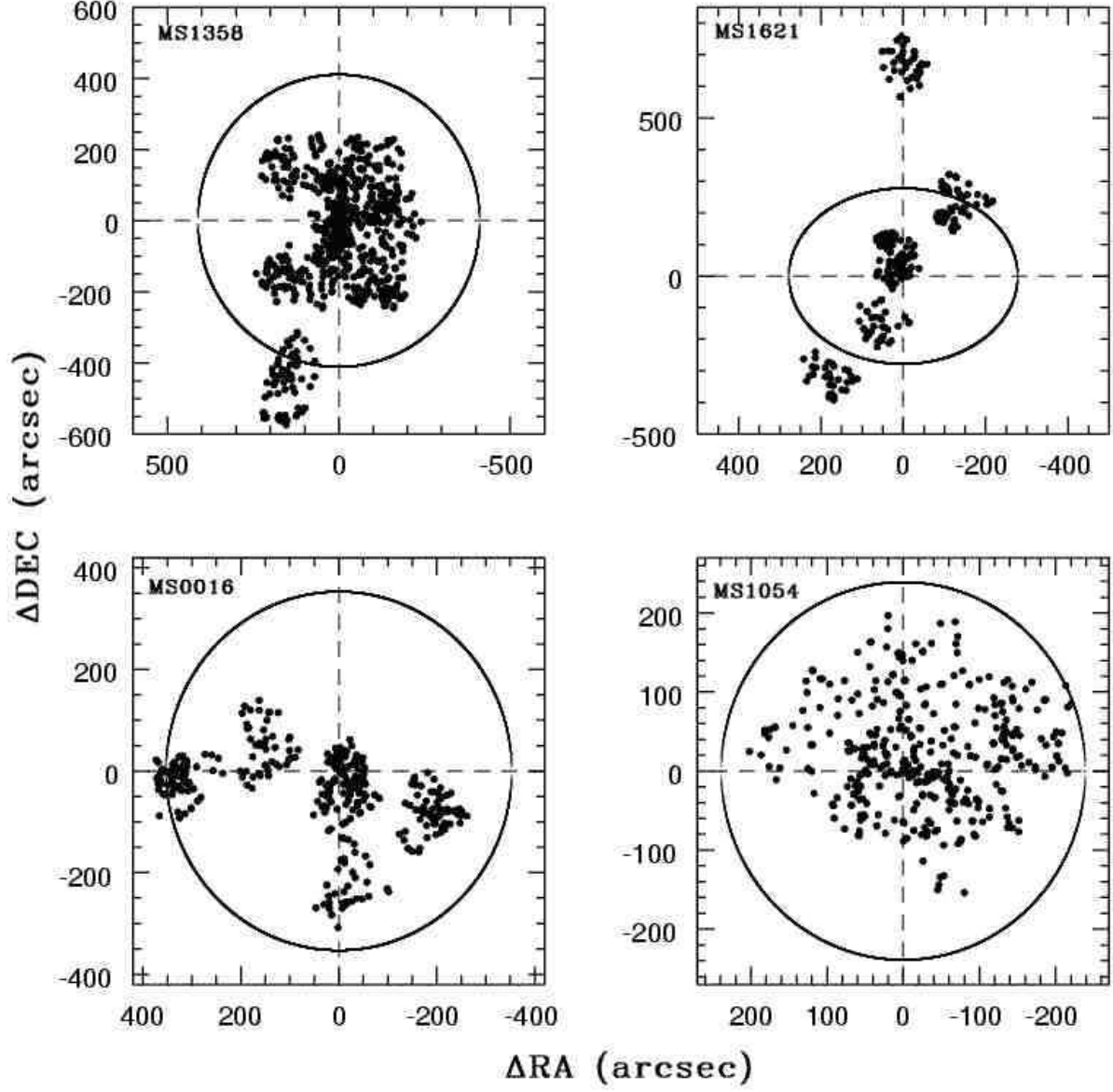


Fig. 1.— Spatial distribution of the galaxies in the sample. The lines plotted on each frame represent  $r_{200}$ , the characteristic radius of each cluster.

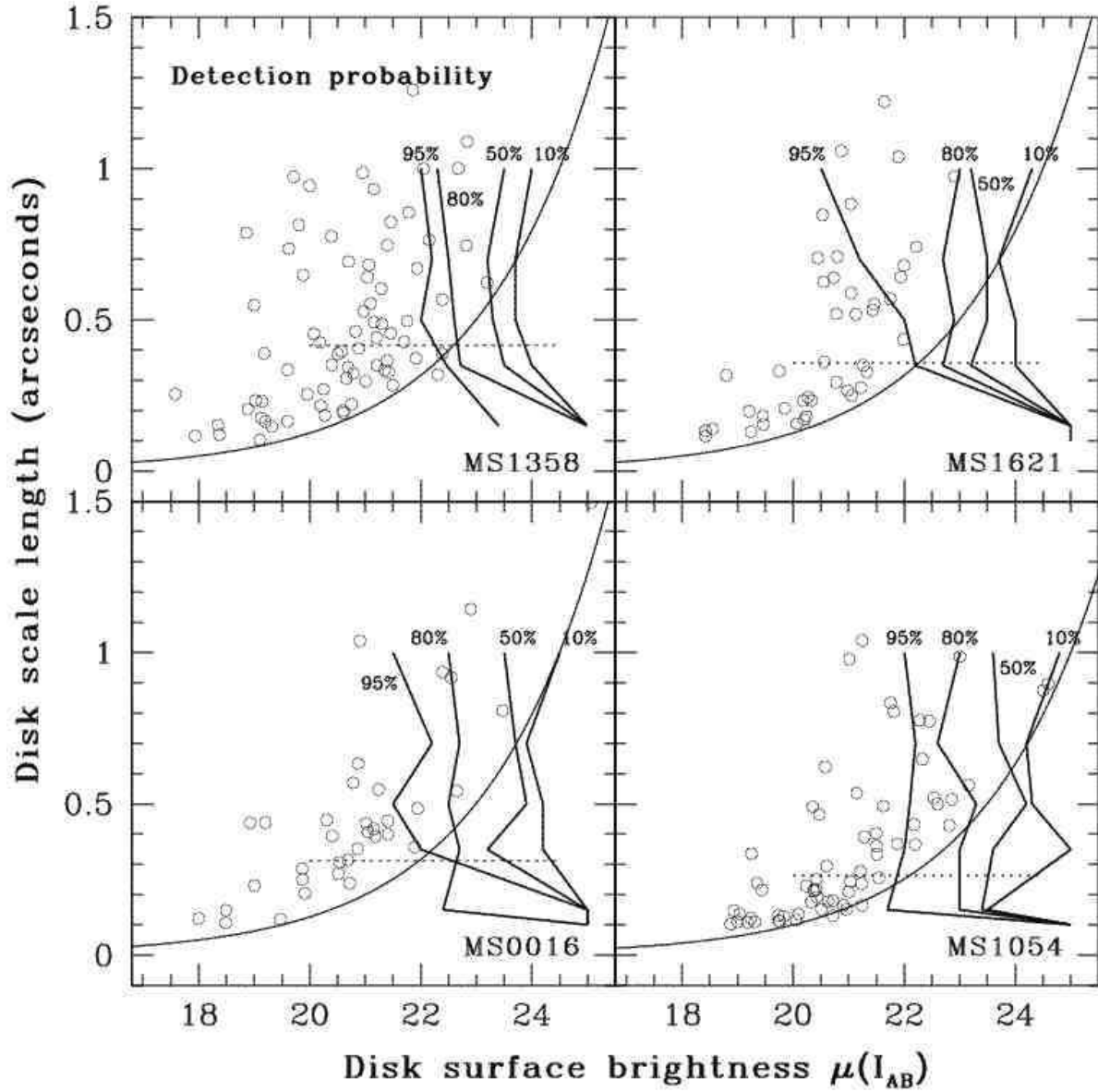


Fig. 2.— Selection probabilities for pure disk galaxies in the four clusters.

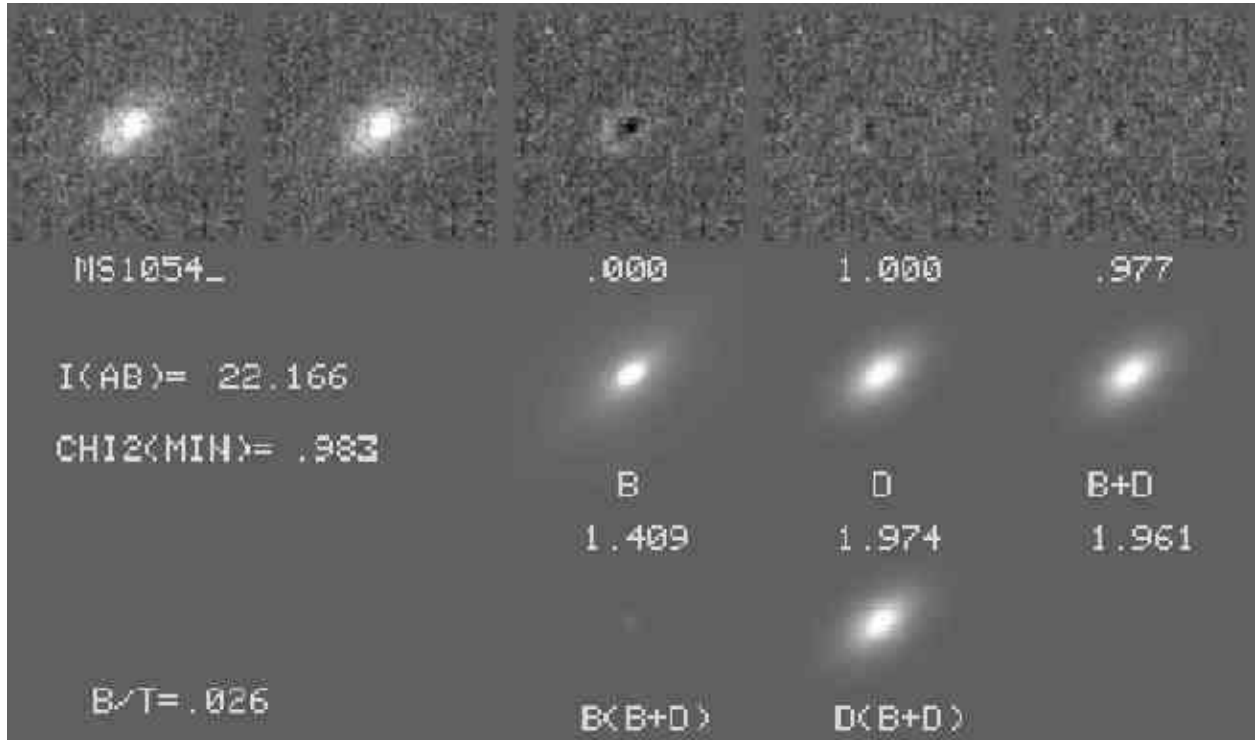


Fig. 3.— The image display used to evaluate the results of the model-fitting procedure. The top row (left-to-right) shows the original image, the "symmetrized" image, and the residuals after the best-fitting bulge,disk, and bulge-plus-disk model is subtracted from the original image. More details are in the text.

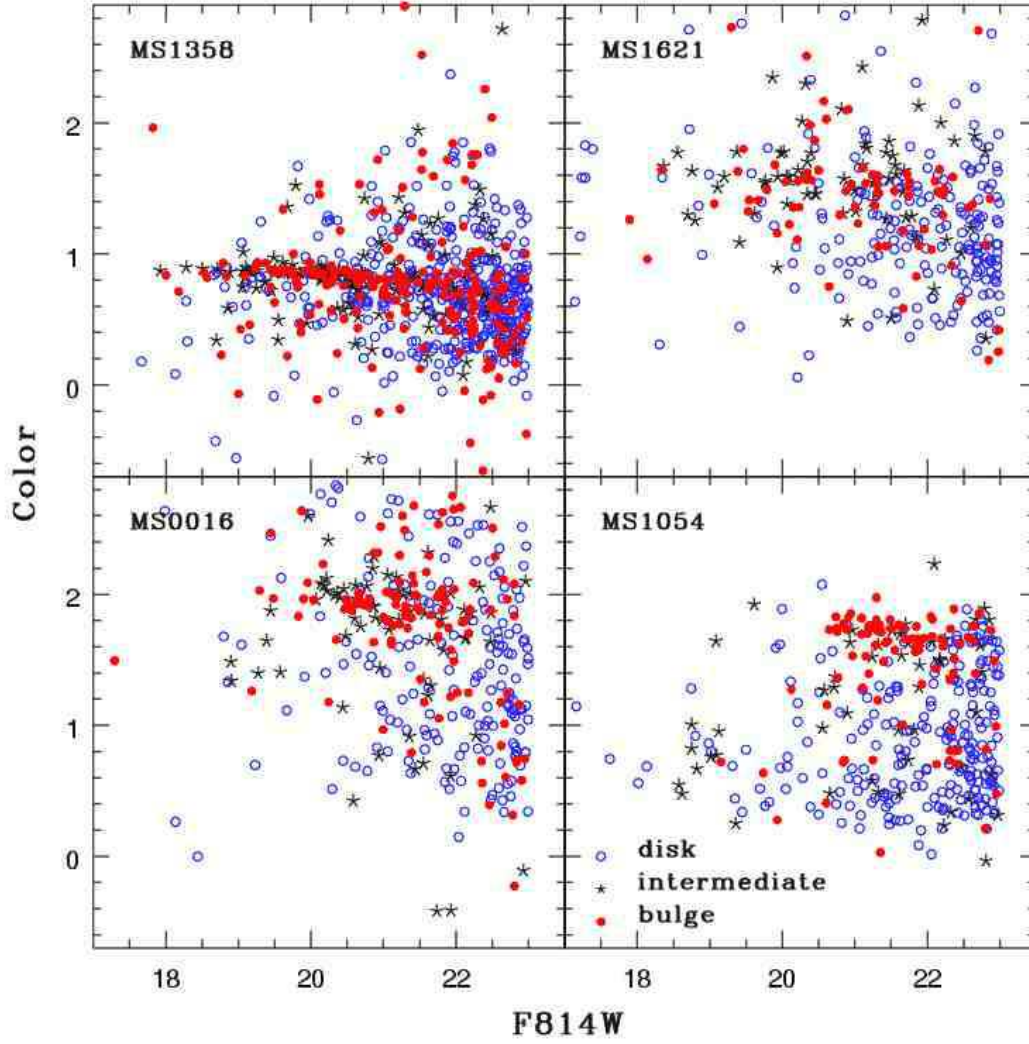


Fig. 4.— Color-magnitude relation for each cluster. Color is  $(F814W-F555W)$  for clusters MS1621 and MS0016 and  $(F814W-F606W)$  for MS1358 and MS1054, and the magnitude is the total observed in the F814W band.

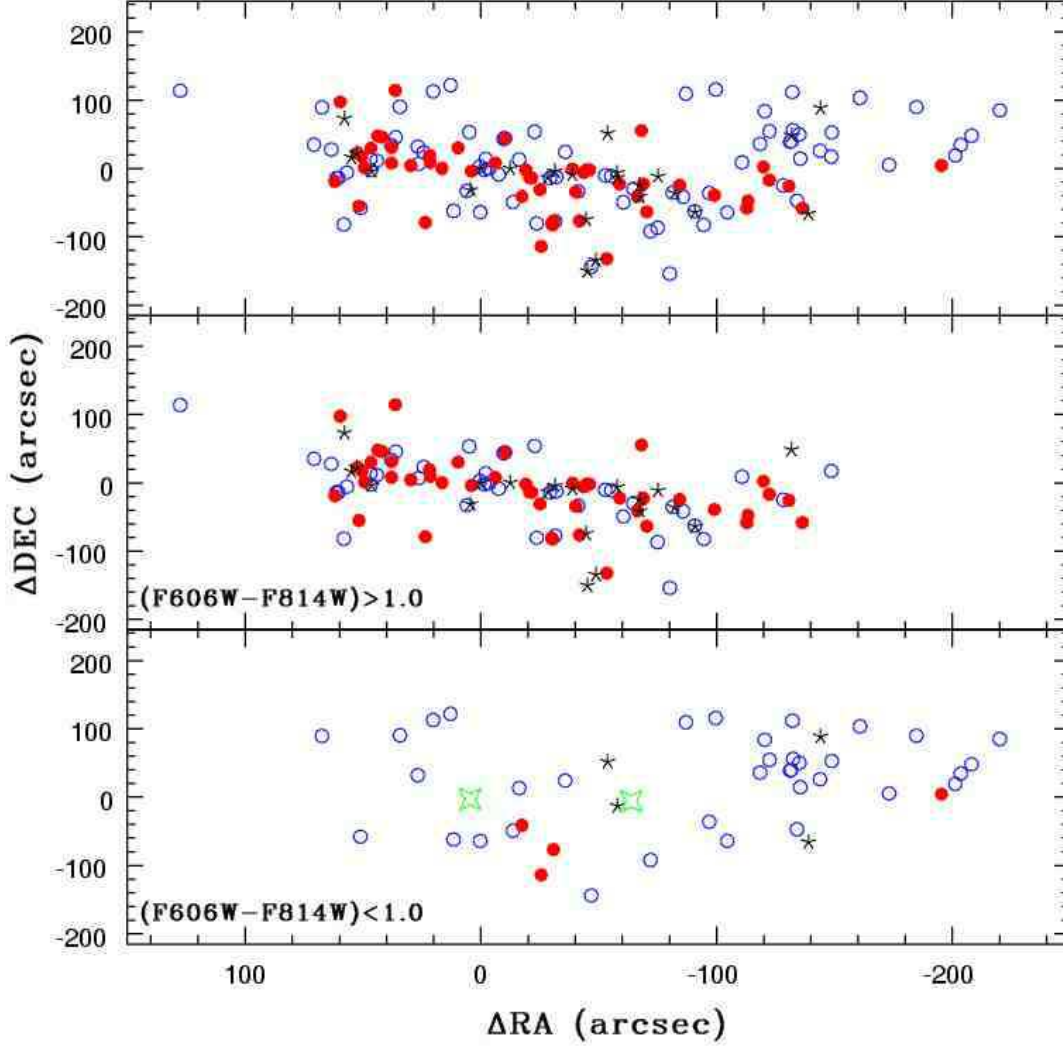


Fig. 5.— Spatial distribution of the galaxies in MS1054 by galaxy type. Open circles are disk galaxies, filled circles bulge galaxies, and stars intermediate galaxies. The top panel presents all galaxies from the data set with  $F814W \leq 23.0$ , the bottom panels show the two groups identified on the color-magnitude diagram. The open stars on the third panel are the centers of the high density regions observed in X-ray (Jeltema et al. 2001).

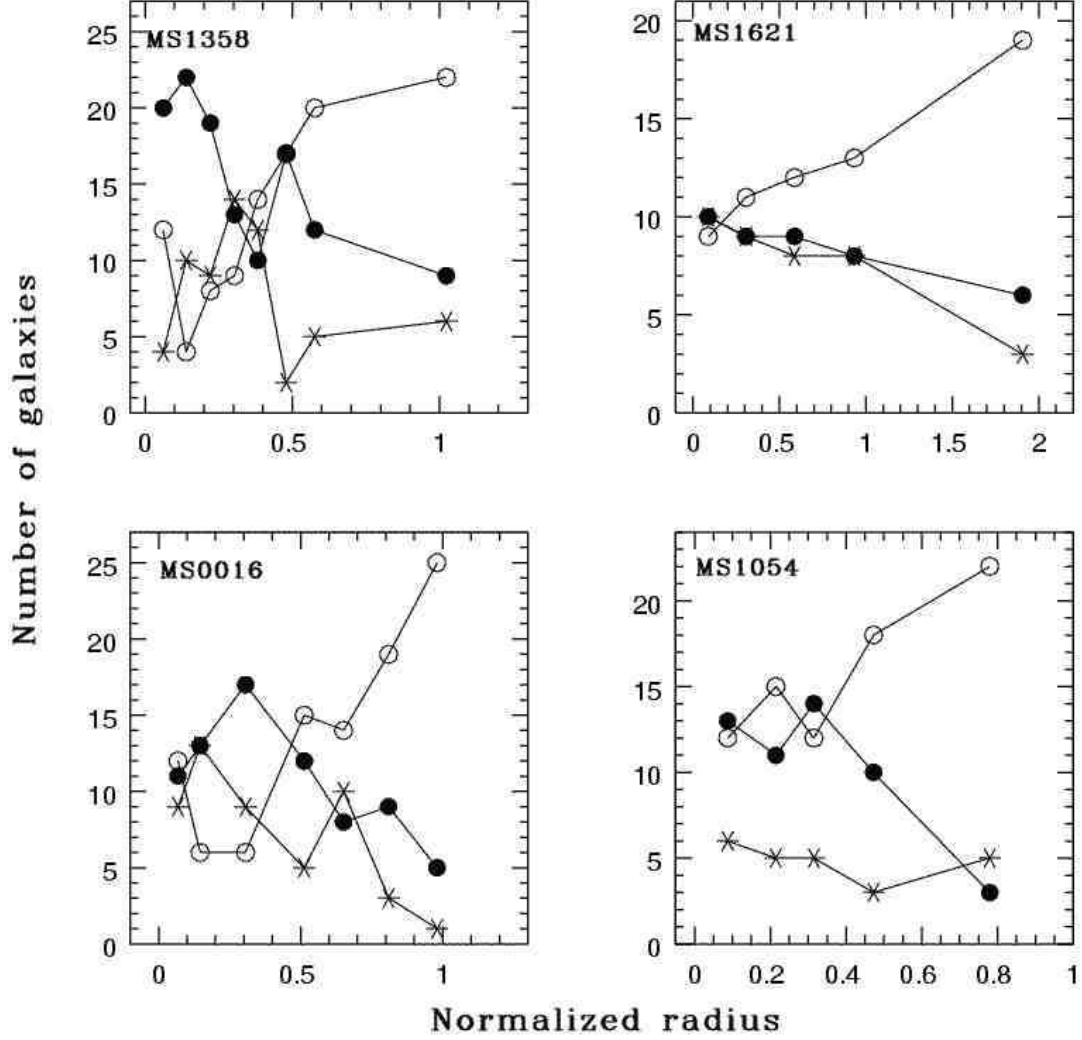


Fig. 6.— Morphology-radius relation for each cluster. For each cluster, the radius bins all contain equal numbers of galaxies. The number of galaxies of each type observed in that bin is normalized by that total. Disk galaxies ( $0 \leq B/T \leq 0.4$ ) are represented by open circles, bulges ( $0.8 \leq B/T \leq 1$ ) by filled circles and intermediate galaxies ( $0.4 < B/T < 0.8$ ) by stars.

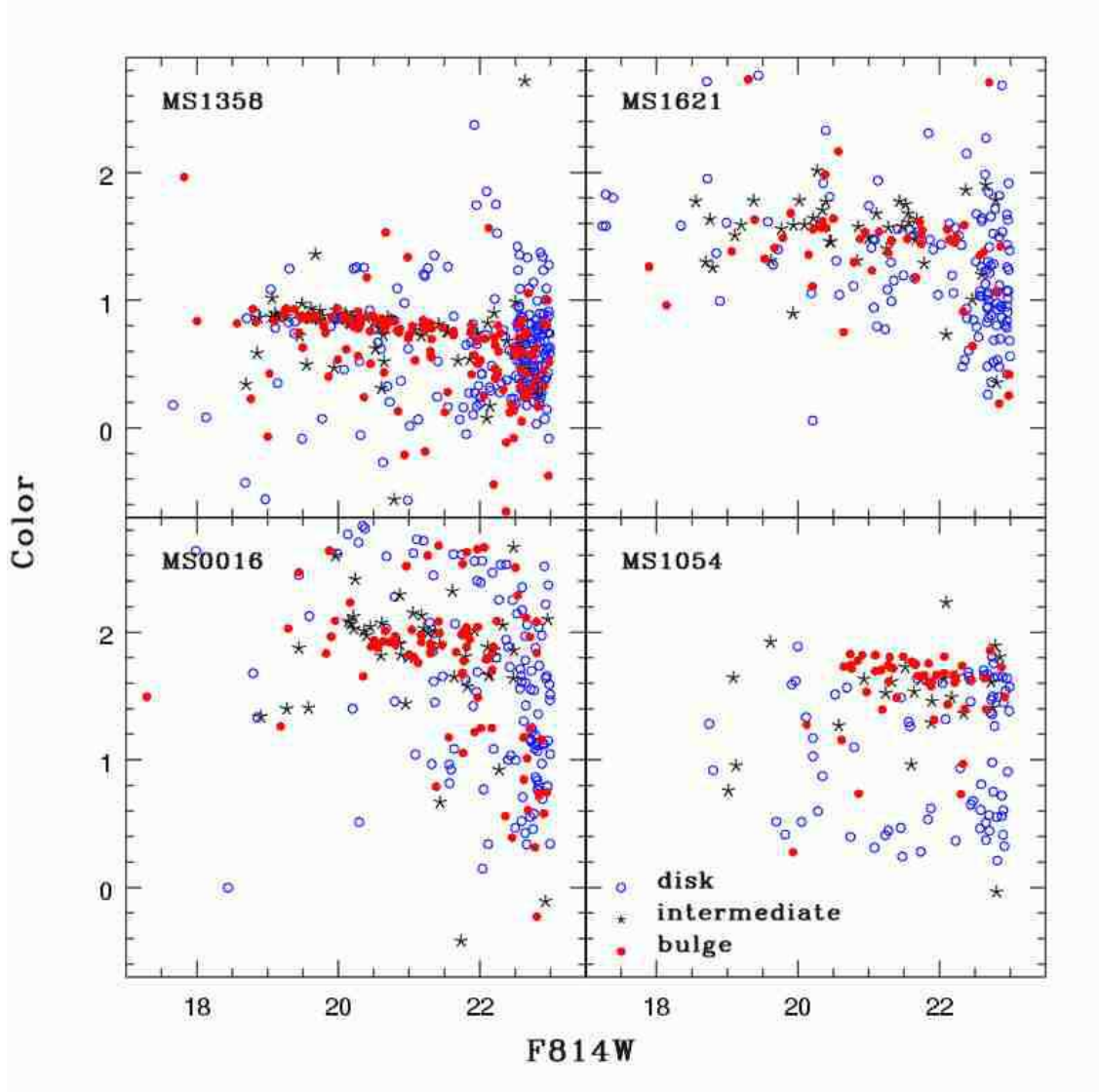


Fig. 7.— Color-Magnitude relation, after the field contamination correction is applied. Color is  $(F814W-F555W)$  for clusters MS1621 and MS0016 and  $(F814W-F606W)$  for MS1358 and MS1054. Open circles represent disk galaxies, stars intermediate galaxies, and filled circles bulge-dominated galaxies.

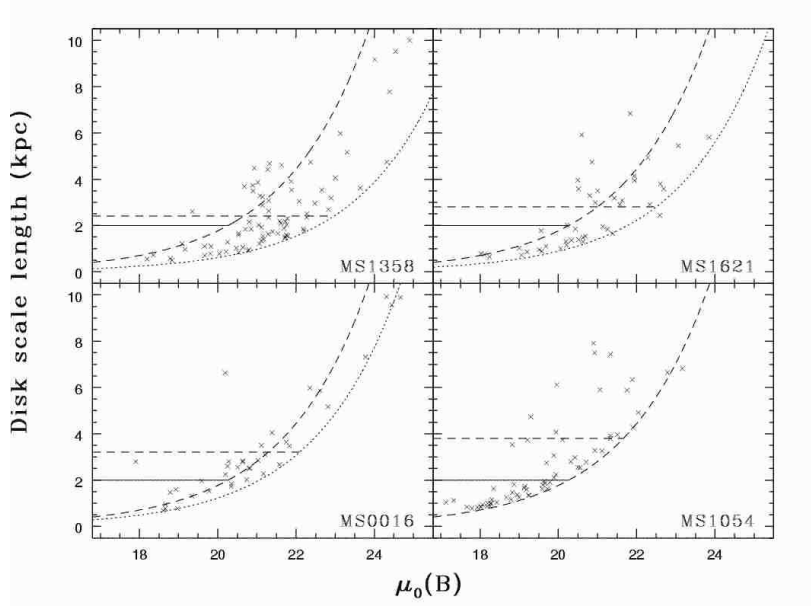


Fig. 8.— Relation between the disk scale length and rest-frame B disk surface brightness for the 4 clusters. In each panel the selection line due to the limiting magnitude ( $F814W(AB) < 22.5$  for MS1358, MS1621 and MS0016) is indicated by a dotted, curved line, and the corresponding line for MS1054 ( $F814W(AB) < 23.0$ ) is shown on all panels as a dashed curve. A horizontal dashed line indicates the angular size of 0.5 arcseconds where incompleteness starts to become significant. We also indicate 2 kpc by a solid line. Below 2 kpc the samples of disk galaxies are complete to the nominal limiting magnitude. Below 2 kpc and to the left of the limiting magnitude dashed line for MS1054 all of the clusters are complete so that the disk populations can be directly compared.

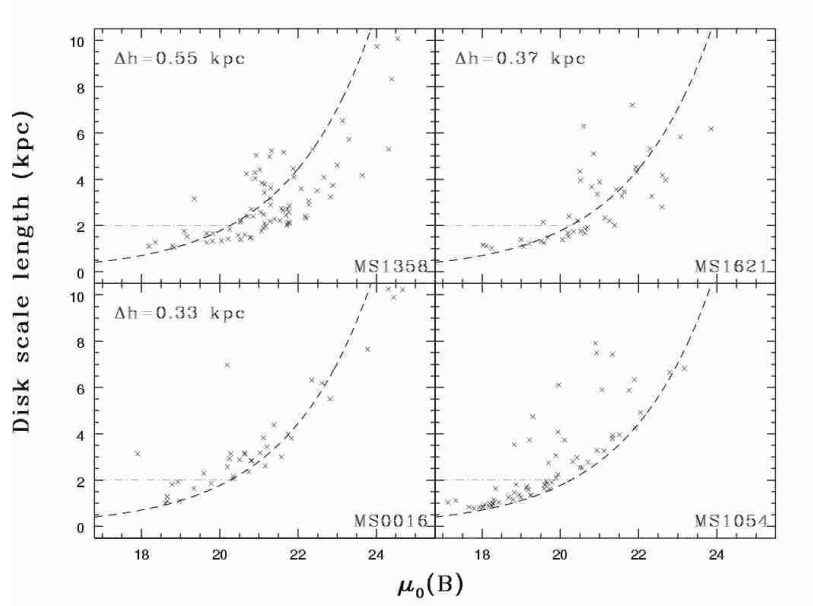


Fig. 9.— Testing the size evolution hypothesis: the size distribution of each cluster is shifted so that the same expected number of galaxies is present above the selection line and below the 2 kpc horizontal line. The model fails in the case of MS1358 and MS0016 where it cannot provide the number of expected disks. Surface brightness is in the rest-frame B(AB).

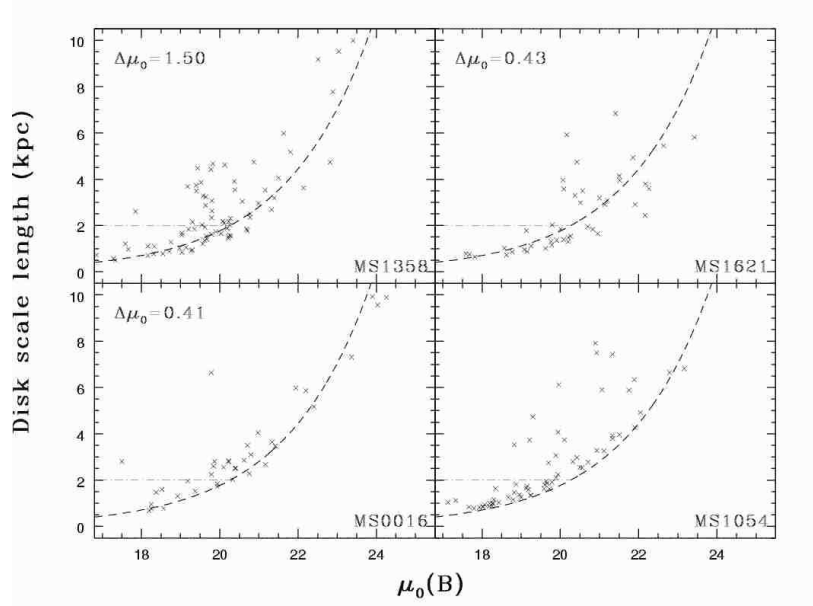


Fig. 10.— Estimation of the shift in the surface brightness distribution. The surface brightness distribution has been shifted until the same expected number of galaxies was above the selection line and below the 2 kpc horizontal line. The shift in surface brightness required is indicated in each frame. Surface brightness is in the rest-frame B(AB).

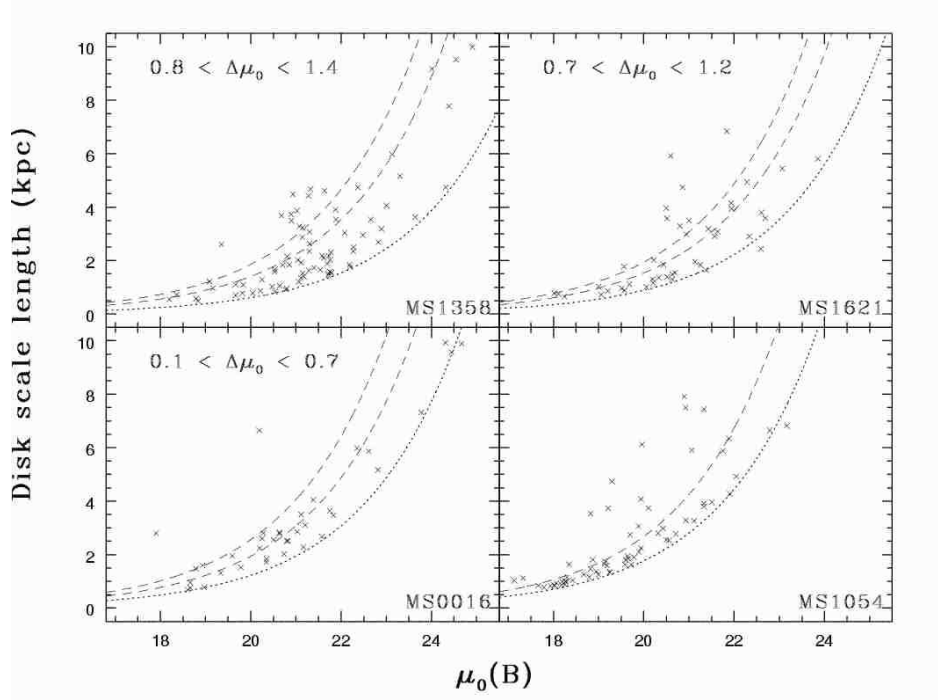


Fig. 11.— Estimation of the surface brightness enhancement with redshift. Lower and higher estimates of the position of the upper limit of the distribution are plotted as the dashed lines. The dotted line represents the faint magnitude limit for each cluster. The ranges for the shifts in surface brightness from MS1054 are indicated in each frame.



Fig. 12.— An example of the fits to a very small galaxy with  $I(AB) = 22.56$  in MS1054. The arrangement of the images in the top row are as discussed in Figure 3 and show that we can distinguish statistically between bulge and disk models even where the derived disk scale length is very small ( $h = 0.108$  arcseconds). Note that the light profile, convolved with the point-spread function can be traced over many pixels although the scale length is only slightly larger than 1 pixel.

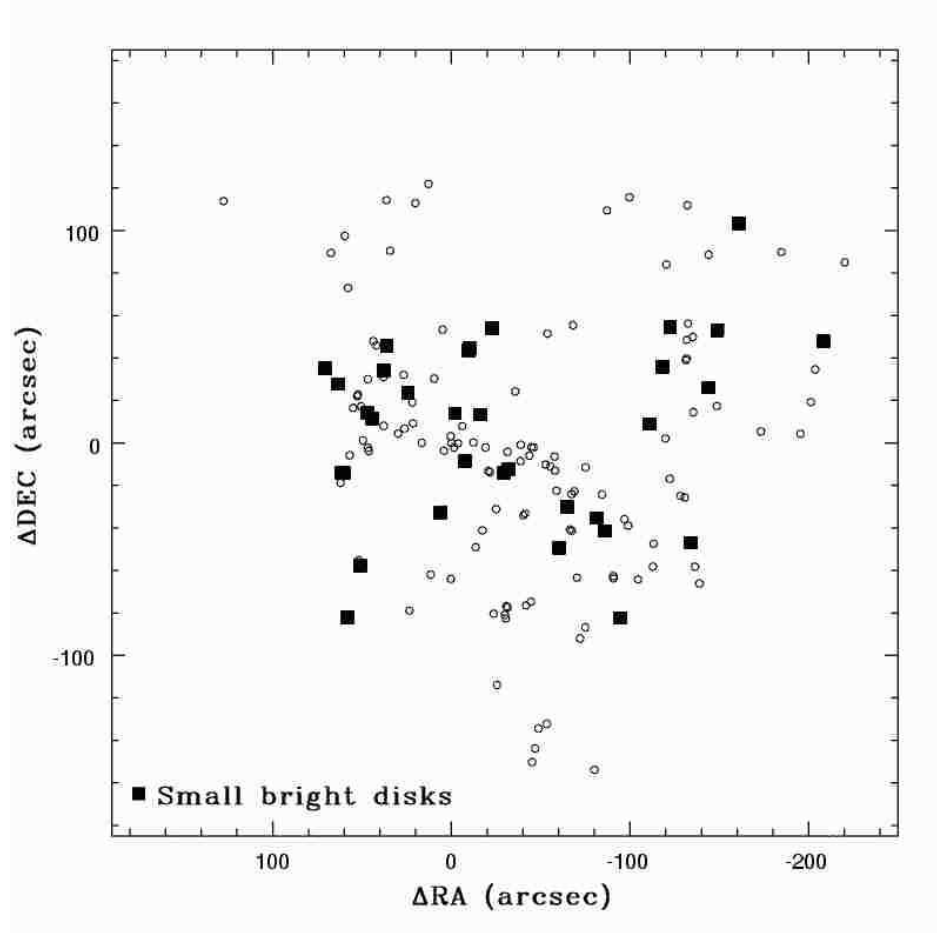


Fig. 13.— Distribution of the small ( $h \leq 2$  kpc), high surface brightness disks in MS1054. The filled squares represent these small disks and the open circles the remaining galaxies of the sample.

Table 2. Catalog of MS 0015.9+1609

Name	$\alpha_{J2000}$ (2)	$\delta_{J2000}$ (3)	Mag (4)	<i>Color</i> <sup>1</sup> (5)	<i>z</i>	B/T (6)	$\mu_D / \mu_B$ (7)	H / Re (8)	$AR_D / AR_B$ (9)	$PA_D / PA_B$ (10)
A_3_2221_0816	00 18 20.9	16 24 52.2	21.054	3.392	...	0.08	24.610	$2.8 \pm 2.7$	$0.49 \pm 0.45$	8.9
A_4_5402_5249	00 18 21.0	16 26 12.9	21.594	0.924	0.385	0.	15.108	$0.30 \pm 0.09$	$0.37 \pm 0.08$	44.8
B_2_5983_7213*	00 18 33.7	16 21 7.9	21.949	2.753	...	1.	21.238	$0.55 \pm 0.03$	$0.38 \pm 0.02$	323.0
B_4_6632_6691*	00 18 32.3	16 24 1.3	21.034	1.403	...	0.27	15.953	$0.95 \pm 0.06$	$0.42 \pm 0.02$	108.9
C_2_0562_0892*	00 18 45.3	16 27 7.3	21.870	0.671	...	0.20	20.741	$0.32 \pm 0.02$	$0.89 \pm 0.04$	328.5
C_3_1549_4203	00 18 43.0	16 27 24.1	20.216	2.123	0.554	0.56	16.595	$1.21 \pm 0.19$	$0.29 \pm 0.04$	92.2
D_3_1695_7261*	00 18 59.2	16 25 39.9	21.888	1.906	...	0.	21.389	$0.39 \pm 0.02$	$0.55 \pm 0.03$	91.1
D_4_1038_3508	00 18 54.5	16 25 3.5	20.296	0.513	...	0.26	14.411	$0.28 \pm 0.05$	$0.25 \pm 0.05$	3.4
E_1_5836_6117	00 18 36.0	16 25 59.1	20.800	1.907	0.554	1.	19.777	$0.48 \pm 0.02$	$0.20 \pm 0.01$	355.0
E_3_0524_6061	00 18 30.2	16 26 8.6	20.985	1.802	0.544	0.77	12.199	$0.21 \pm 0.01$	$0.74 \pm 0.04$	2.2
							23.572	$1.15 \pm 0.06$	$0.57 \pm 0.03$	3.7
							19.202	$0.44 \pm 0.02$	$0.22 \pm 0.01$	330.2
							21.617	$20.0 \pm 8.4$	$0.21 \pm 0.02$	158.1
							14.876	$0.44 \pm 0.02$	$0.93 \pm 0.05$	76.2
							20.313	$0.21 \pm 0.01$	$0.46 \pm 0.02$	356.1
							12.558	$0.22 \pm 0.01$	$0.66 \pm 0.03$	222.8

<sup>1</sup>Color is (F814W-F555W)

Note. — The complete version of this table is in the electronic edition of the Journal. The printed edition contains only a sample.

Table 3. Catalog of MS 1054.4-0321

Name	$\alpha_{J2000}$ (2)	$\delta_{J2000}$ (3)	Mag (4)	<i>Color</i> <sup>1</sup> (5)	B/T (6)	$\mu_D / \mu_B$ (7)	H / Re (8)	$AR_D / AR_B$ (9)	$PA_D / PA_B$ (10)
A_2_5257_2843	10 56 48.4	-03 37 31.1	20.282	0.598	0.02	24.019	$2.6 \pm 2.0$	$0.75 \pm 0.39$	200.4
A_4_1255_5906*	10 56 53.7	-03 36 35.6	22.723	1.318	0.	12.274	$0.05 \pm 0.03$	$0.44 \pm 0.22$	122.1
B_2_7326_1845	10 56 53.6	-03 38 58.9	22.086	1.318	0.22	20.26	$0.16 \pm 0.01$	$0.61 \pm 0.03$	345.2
B_4_4364_4854	10 56 57.5	-03 37 12.3	21.277	0.447	0.	20.235	$0.23 \pm 0.01$	$0.43 \pm 0.02$	85.5
C_3_5770_5963*	10 56 55.7	-03 38 5.7	21.423	1.631	1.	17.405	$0.82 \pm 0.18$	$0.41 \pm 0.11$	16.6
D_4_2364_4815*	10 57 11.7	-03 37 30.6	22.312	0.962	0.18	21.142	$0.54 \pm 0.03$	$0.49 \pm 0.02$	304.3
E_2_1561_2215	10 57 2.7	-03 36 50.6	21.956	1.665	1.	15.224	$0.64 \pm 0.03$	$0.76 \pm 0.04$	179.0
E_3_4427_6160	10 57 1.3	-03 35 43.6	21.234	0.411	0.11	21.315	$0.27 \pm 0.01$	$0.73 \pm 0.04$	7.7
F_2_5849_3682*	10 56 57.3	-03 36 23.9	21.177	1.011	0.01	14.989	$0.16 \pm 0.09$	$0.78 \pm 0.21$	297.4
F_4_2673_1801*	10 57 0.4	-03 35 8.3	22.295	0.706	0.11	14.445	$0.34 \pm 0.02$	$0.83 \pm 0.04$	97.4
						21.013	$0.98 \pm 0.05$	$0.12 \pm 0.01$	36.8
						16.265	$0.44 \pm 0.13$	$0.58 \pm 0.10$	24.1
						21.334	$0.51 \pm 0.03$	$0.71 \pm 0.04$	12.2
						12.001	$0.02 \pm 0.03$	$0.5 \pm 1.3$	273.0
						24.273	$2.7 \pm 6.2$	$0.12 \pm 0.25$	335.3
						16.514	$0.43 \pm 0.23$	$0.26 \pm 0.06$	174.4

<sup>1</sup>Color is (F814W-F606W)

Note. — The complete version of this table is in the electronic edition of the Journal. The printed edition contains only a sample.

Table 4. Catalog of MS 1358.4+6245

Name	$\alpha_{J2000}$ (2)	$\delta_{J2000}$ (3)	Mag (4)	<i>Color</i> <sup>1</sup> (5)	<i>z</i>	B/T (6)	$\mu_D / \mu_B$ (7)	H / Re (8)	$AR_D / AR_B$ (9)	$PA_D / PA_B$ (10)
A_2_5725_2798	13 59 48.3	62 31 57.8	20.511	0.839	0.322	0.75	20.192	$0.34 \pm 0.02$	$0.24 \pm 0.01$	176.3
A_4_0726_5554	13 59 46.3	62 30 25.9	20.172	0.842	0.334	1.	12.465	$0.33 \pm 0.02$	$0.40 \pm 0.02$	174.3
B_2_4601_2187*	13 59 34.4	62 31 47.1	21.977	0.633	...	0.	12.166	$0.31 \pm 0.02$	$0.61 \pm 0.03$	15.3
D_4_5092_2352	13 59 32.3	62 27 42.4	17.664	0.179	0.328	0.23	20.353	$0.23 \pm 0.01$	$0.70 \pm 0.03$	332.8
							25.007	$29.9 \pm 6.7$	$0.12 \pm 0.28$	107.5
F_2_4360_5659	13 59 59.8	62 29 33.7	19.203	0.886	0.337	0.61	11.552	$0.34 \pm 0.02$	$0.65 \pm 0.03$	245.8
							20.473	$0.50 \pm 0.02$	$0.80 \pm 0.04$	85.1
G_3_7214_0725*	14 00 19.9	62 29 16.1	20.875	1.317	0.532	0.89	12.816	$0.46 \pm 0.02$	$0.75 \pm 0.04$	80.0
							20.762	$0.22 \pm 0.01$	$0.33 \pm 0.03$	108.6
I_3_7580_4164	14 00 9.7	62 34 4.2	22.487	0.577	...	0.	13.556	$0.47 \pm 0.02$	$0.44 \pm 0.02$	105.4
J_2_7234_6432*	14 00 8.2	62 25 51.8	21.527	2.396	...	0.	22.383	$0.39 \pm 0.02$	$0.96 \pm 0.05$	87.1
L_2_4827_1935*	13 59 41.2	62 34 20.8	21.094	0.456	0.382	0.14	19.627	$0.32 \pm 0.02$	$0.28 \pm 0.01$	80.5
							20.890	$0.41 \pm 0.02$	$0.68 \pm 0.03$	75.8
M_3_5846_7043	13 59 41.6	62 33 30.4	20.699	0.870	...	0.63	19.075	$2.34 \pm 0.19$	$0.37 \pm 0.03$	100.1
							23.288	$1.51 \pm 0.23$	$0.28 \pm 0.04$	222.5
							15.682	$1.13 \pm 0.08$	$0.45 \pm 0.02$	178.1

<sup>1</sup>Color is (F814W-F606W) except for galaxies with names starting with J or K, in which case it is (F814W-F450W)

Note. — The complete version of this table is in the electronic edition of the Journal. The printed edition contains only a sample.

Table 5. Catalog of MS 1621.5+2640

Name	$\alpha_{J2000}$ (2)	$\delta_{J2000}$ (3)	Mag (4)	<i>Color</i> <sup>1</sup> (5)	<i>z</i>	B/T (6)	$\mu_D / \mu_B$ (7)	H / Re (8)	$AR_D / AR_B$ (9)	$PA_D / PA_B$ (10)
A_1_3143_6511	16 23 39.7	26 35 2.8	21.569	1.609	...	0.48	20.581	$0.27 \pm 0.01$	$0.20 \pm 0.01$	339.7
							13.672	$0.13 \pm 0.01$	$0.81 \pm 0.04$	124.7
A_3_2629_2271	16 23 35.5	26 35 9.6	21.635	1.510	...	0.	22.906	$0.97 \pm 0.06$	$0.54 \pm 0.03$	60.2
B_2_0999_0800	16 23 40.8	26 31 35.1	21.432	1.774	...	0.60	20.605	$0.19 \pm 0.01$	$0.85 \pm 0.04$	74.4
							15.181	$0.47 \pm 0.03$	$0.81 \pm 0.06$	8.1
B_3_0615_2903*	16 23 39.4	26 31 57.5	21.307	1.526	...	1.	12.868	$0.37 \pm 0.02$	$0.30 \pm 0.01$	118.0
C_2_1460_4198	16 23 24.9	26 37 38.0	19.062	1.384	0.431	0.95	23.377	$0.80 \pm 0.04$	$0.72 \pm 0.04$	8.1
							16.154	$2.66 \pm 0.13$	$0.87 \pm 0.04$	173.2
C_4_1317_2943	16 23 27.3	26 38 36.0	20.646	0.750	...	1.	19.386	$6.56 \pm 0.40$	$0.69 \pm 0.03$	3.8
D_2_2851_6055*	16 23 48.9	26 27 50.4	21.859	1.518	...	0.25	21.715	$0.40 \pm 0.02$	$0.67 \pm 0.03$	92.2
							13.063	$0.11 \pm 0.02$	$0.56 \pm 0.09$	45.3
D_3_0732_3391*	16 23 48.9	26 29 5.4	21.713	1.052	...	0.33	20.519	$0.29 \pm 0.01$	$0.43 \pm 0.02$	29.0
							16.167	$1.12 \pm 0.10$	$0.15 \pm 0.02$	36.4
E_2_7010_6640	16 23 35.9	26 43 40.5	20.393	2.329	...	0.	18.798	$0.32 \pm 0.02$	$0.36 \pm 0.02$	105.2
E_3_3666_2448*	16 23 33.0	26 45 1.1	19.888	1.216	0.393	0.14	20.218	$0.54 \pm 0.03$	$0.63 \pm 0.03$	95.0
							11.023	$0.12 \pm 0.01$	$0.25 \pm 0.01$	29.0

<sup>1</sup>Color is (F814W-F555W)

Note. — The complete version of this table is in the electronic edition of the Journal. The printed edition contains only a sample.

Table 6. Normalization factor

Cluster	$f_m$ <sup>1</sup>	$f_g$ <sup>2</sup>
MS 1358+62	0.657	0.477
MS 1621+26	0.314	0.161
MS 0016+16	0.312	0.273
MS 1054-03	0.846	1.00

<sup>1</sup>Fractions of the cluster mass observed, using the density profile of Carlberg et al. (1997b)

<sup>2</sup>Fractions of the cluster galaxies observed, normalized to MS1054. Factors calculated with the cluster masses from Carlberg et al. (1996) and Tran et al. (1999) for MS1054. These are the fraction of the cluster observed weighted by the mass of the clusters.

Table 7. Results of Evolution Models

Cluster	N <sup>1</sup>	$\Delta h$	$\Delta\mu_0$ <sup>2</sup>	$\Delta\mu_0(95\%)$ <sup>3</sup>	med < $h$ > <sup>4</sup>	$\sigma_h$	$\Delta\mu_0$ (env) <sup>5</sup>
MS 1358+62	15	0.55	1.50	0.70—1.76	1.40	0.41	0.8-1.4
MS 1621+26	5	0.37	0.43	0.0—0.87	1.14	0.54	0.7-1.2
MS 0016+16	9	0.33	0.41	0.0—0.80	1.53	0.30	0.1-0.7
MS 1054-03	33	...	...	...	1.29	0.38	...

<sup>1</sup>“Equivalent” number of small bright disks used for each cluster. They were calculated with the normalization factors and based on the count of 33 small bright disks in MS1054

<sup>2</sup>Shift required in the surface brightness as determined by the counts normalization technique and its 95% confidence interval.

<sup>3</sup>The 95% confidence interval in the surface brightness shift.

<sup>4</sup>Median of the size distribution of the small bright disks after the shift in surface brightness, also the standard deviation of that distribution

<sup>5</sup>Range for the shift in the surface brightness evaluated with the upper envelope technique.